Post-Golgi anterograde transport requires GARP-dependent endosome-to-TGN retrograde transport

Tetsuya Hirata

2016.3

1. Table of contents

2. Abstract

Glycosylphosphatidylinositol (GPI) anchoring of proteins is an evolutionarily conserved post-translational modification. In mammalian cells, over 100 proteins are anchored by GPI to the cell surface. The biosynthesis of GPI is carried out in the ER, generating precursor of GPI-anchored proteins. Precursors then undergo structural remodeling of GPI to generate mature GPI-anchored proteins. The molecular mechanisms of the post-Golgi transport of GPI-anchored proteins are not well understood. For example, whether GPI-anchored proteins require transmembrane cargo receptors or not is still unresolved. To address these issue, I took advantage of forward genetic screening using human haploid cell line, HAP1 cell, and identified subunits of the Golgi-associated retrograde protein (GARP) complex, a tethering factor involved in endosome-to-TGN retrograde transport. Knockout (KO) of each of the four GARP subunits, VPS51-VPS54, in HEK293 cells caused severely defective anterograde transport of both GPI-anchored and transmembrane proteins from the TGN. Overexpression of VAMP4, v-SNARE, in VPS54-KO cells partially restored not only endosome-to-TGN retrograde transport, but also anterograde transport of both GPI-anchored and transmembrane proteins. Further screening for genes whose overexpression rescue the VPS54-KO phenotype identified TMEM87A, encoding an uncharacterized Golgi-resident membrane protein. Overexpression of TMEM87A or its close homologue TMEM87B in VPS54-KO cells partially restored endosome-to-TGN retrograde transport and anterograde transport. Therefore, post-Golgi anterograde transport is coupled with endosome-to-TGN retrograde transport for recycling of molecules critical for efficient post-Golgi anterograde transport of membrane proteins. In addition, TMEM87A and TMEM87B are involved in endosome-to-TGN retrograde transport.

3. General introduction

Protein trafficking in eukaryotic cells is mediated by bidirectional vesicular transport between cellular compartments (Brandizzi and Barlowe, 2013). Vesicular transport can be divided into two pathways: anterograde transport, which is the route from the ER to the plasma membrane, and retrograde transport, which is the opposite route. Each of these transport pathways consists of four steps; budding, movement, tethering, and uncoating and fusion (Bonifacino and Glick, 2004; Brandizzi and Barlowe, 2013). Anterograde transport from the ER to the ERGIC-Golgi is mediated by COPII-coated vesicles, and retrograde transport from the Golgi to the ER by COPI-coated vesicles. Abnormality of COPI-dependent retrograde transport from the ERGIC disrupts COPII-mediated anterograde transport from the ER since recycling of proteins, such as v-SNAREs and cargo receptors, is disturbed (Pepperkok *et al.*, 1993; Peter *et al.*, 1993). Therefore, protein recycling mediated by COPI-dependent retrograde transport is required for efficient anterograde transport from the ER. Anterograde and retrograde transport also take place between the TGN and the plasma membrane. Three retrograde transport pathways to the TGN have been identified: from early, recycling, or late endosomes (Chia *et al.*, 2013). Fusion of endosome-derived retrograde carriers with the TGN membrane is mediated by SNARE complex assembly between v-SNARE, vesicle-associated membrane protein 4 (VAMP4), and the TGN-localized t-SNAREs, Syntaxin 6 (STX6), STX16 and Vti1 (Mallard *et al.*, 2002; Hong and Lev, 2013). Retrograde transport to the TGN was first discovered through the transport routes of toxins (Mallard *et al.*, 1998) and is now thought to act as a protein recycling route from endosomes.

Glycosylphosphatidylinositol (GPI) anchoring of proteins is an evolutionarily

conserved post-translational modification (Kinoshita *et al.*, 2008). In mammalian cells, over 100 proteins are anchored by GPI to the cell surface. GPI is a glycolipid composed of phosphatidylinositol, glucosamine, 3 mannoses (Mans) and 2 ethanolamine phosphates (EtNPs) and attached to the C-terminus of proteins (Fig. 1A). The biosynthesis of GPI is carried out in the ER, generating precursor of GPI-anchored proteins (GPI-APs) (Fig. 1B). The precursors are remodeled in their sugar and the lipid portion in the ER and the Golgi. The remodeling of GPI in the ER is carried out by post-GPI attachment to proteins 1 (PGAP1) and PGAP5 (Tanaka *et al.*, 2004; Fujita *et al.*, 2009). PGAP1 removes acyl chain linked to the inositol and PGAP5 removes EtNP on the 2nd Man (Fig. 1C). Remodeled GPI-APs are then accumulated in the ER exit site in the p24 family complex dependent manner, a cargo receptor of GPI-APs (Fujita *et al.*, 2011), and transported to the Golgi mediated by COPII vesicles (Fig. 1C). GPI-APs in the Golgi undergo fatty acid remodeling mediated by PGAP3 and PGAP2 (Tashima *et al.*, 2006; Maeda *et al.*, 2007). PGAP3 removes unsaturated fatty acid from the sn2 position and PGAP2 is essential for addition of a saturated fatty acid, usually stearic acid, to the same position, resulting in mature GPI-APs (Fig. 1C). Lipid moiety of mature GPI-APs bearing saturated fatty acid chains is compatible with lipid microdomains, termed lipid-rafts that are enriched in glycoshingolipid and cholesterol. In fact, GPI-APs are major proteins in lipid-rafts.

The molecular mechanisms for the anterograde transport of GPI-APs from the ER is relatively well understood. Because GPI-APs lack cytoplamic domain, they cannot directly bind to the COPII coat proteins and require transmembrane cargo receptors. A complex of p24 family proteins acts as a cargo receptor of GPI-APs by binding to them after they are remodeled by PGAP1 and PGAP5 and concentrates them into ER-exit site.

PGAP1- or PGAP5-defective mutant cells show delayed anterograde transport of GPI-APs due to a lack of efficient binding of GPI-APs with the p24 family complex (Fujita *et al.*, 2011). p24 family of proteins were identified as components of COPI and COPII coated vesicles (Schimmoller *et al.*, 1995; Belden and Barlowe, 1996). The p24 proteins are type I transmembrane proteins conserved from yeast to mammals (Carney and Bowen, 2004). They have a Golgi dynamics (GOLD) domain and an α-helical region in the luminal side, a single-pass transmembrane domain and a short cytoplamic tail which contains binding motifs for the COPI and COPII coat proteins (Strating and Martens, 2009). Thus, p24 family complex can link GPI-APs to the COPII coat proteins, Sec24C or Sec24D (Bonnon *et al.*, 2010).

p24 family proteins are divided into 4 subfamilies, p24α, p24β, p24γ and p24δ (Dominguez *et al.*, 1998). p24β and p24δ subfamilies have only one member, p24β1 and p24δ1, respectively, whereas p24α subfamily have three members, p24α1-3 (α1 is pseudogene in human) and p24γ subfamily have five members, p24γ1-5. The p24 family complex is composed of each one of 4 subfamilies though their stoichiometry has not been determined (Pastor-Cantizano *et al.*, 2015). Knockdown (KD) of p24δ1 or p24γ2 disturbs the anterograde transport of GPI-APs from the ER (Takida *et al.*, 2008; Theiler *et al.*, 2014). Because KD of other p24γ subfamily members does not delay the anterograde transport of GPI-APs, the complex containing p24γ2 subunit is specifically required for sorting of GPI-APs (Theiler *et al.*, 2014). A juxtamembrane α-helical region of p24γ2 subunit is required for the anterograde transport of GPI-APs, implying its role in binding GPI-anchor (Theiler *et al.*, 2014).

4. Introduction of this thesis

Previous studies showed that secretion of Wnt is dependent on endosome-to-TGN retrograde transport, based on the necessary recycling of its cargo receptor, wntless (Belenkaya *et al.*, 2008; Franch-Marro *et al.*, 2008; Harterink *et al.*, 2011). These results highlighted the importance of protein recycling from endosomes. However, other studies showed that anterograde transport of thermosensitive vesicular stomatitis virus G protein ($VSVG^{tsO45}$, hereafter $VSVG^{ts}$), which is more widely used as a model protein for testing anterograde transport, is not impaired in cells depleted of SNARE proteins involved in endosome-to-TGN retrograde transport (Choudhury *et al.*, 2006; Nishimoto-Morita *et al.*, 2009; Shitara *et al.*, 2013). These results were quite different from the case of Wnt secretion and suggested that protein recycling to the TGN is less important for the anterograde transport of $VSVG^{ts}$. Therefore, the relevance of endosome-to-TGN retrograde transport in the post-Golgi anterograde transport is still controversial.

Previously proposed molecular mechanisms of post-Golgi anterograde transport of GPI-APs are debatable. One is lipid based sorting. As GPI-anchor acts as a sorting signal for the apical membrane, most of GPI-APs are localized in the apical membrane surface. In addition of GPI-APs, specific lipids such as sphingolipids and cholesterol are enriched in the apical membrane (van Meer *et al.*, 1987; Simons and van Meer, 1988). Consistent with this, depletion of sphingolipids and/or cholesterol impaired the apical sorting of GPI-APs (Paladino *et al.*, 2004). However, this lipid based sorting model is still not consensus because GPI-APs with unsaturated fatty acid in PGAP3-defective mutant cells are transported to the plasma membrane with the similar kinetics to remodeled GPI-APs (Jaensch *et al.*, 2014). Other proposed model is

oligomerization-dependent sorting. This model is based on the experiment that the impairment of oligomerization of GPI-APs resulted in the missorting to the basolateral membrane (Paladino *et al.*, 2004; Paladino *et al.*, 2007). This model, however, is also debatable. Because oligomerization of GPI-APs is impaired in PGAP3-defective mutant cells (Seong *et al.*, 2013), transport efficiency of GPI-APs in PGAP3 mutant cells should be decreased. However, transport of GPI-APs is normal in PGAP3 mutant cells as described above (Jaensch *et al.*, 2014). The third one is cargo receptor model. This model, however, has not been well studied because putative cargo receptors have not been identified yet. Thus, post-Golgi anterograde transport of GPI-APs requires transmembrane cargo receptors or not is still unresolved.

In this study, I took advantage of forward genetic screening using human haploid cell line, HAP1 cells, to identify genes necessary for the efficient anterograde transport of GPI-APs and thereby identified genes encoding subunits of the Golgi-associated retrograde protein (GARP) complex. The GARP complex is a multi-subunit tethering factor localized in the TGN and involved in endosome-to-TGN retrograde transport (Bonifacino and Hierro, 2011). It is composed of four subunits, VPS51, VPS52, VPS53, and VPS54, each of which is essential for tethering (Conibear and Stevens, 2000; Siniossoglou and Pelham, 2002; Perez-Victoria *et al.*, 2008; Perez-Victoria *et al.*, 2010a). I demonstrated that depletion of GARP complex causes delayed anterograde transport of proteins. Moreover, I performed screening of genes whose overexpression compensates the requirement of GARP complex and identified a gene, *TMEM87A*. TMEM87A is a multi-transmembrane protein and has a close homolog termed TMEM87B. The function of both TMEM87A and TMEM87B has not been reported. Here, I demonstrate that the GARP- and VAMP4-dependent endosome-to-TGN

retrograde transport is required for recycling of factors necessary for the efficient post-Golgi anterograde transport of cell-surface integral membrane proteins, such as GPI-anchored or transmembrane proteins. Also, TMEM87A and TMEM87B might be involved in the endosome-to-TGN retrograde transport.

5. Materials and methods

Reagents and antibodies

Lipofectamine 2000 and Lipofectamine RNAi MAX were purchased from Life Technologies. As primary antibodies, mouse monoclonal anti-CD59 (clone 5H8), anti-FLAG (clone M2), anti-HA (clone HA7) (Sigma-Aldrich), anti-STX6 (Stressgen), anti-α-tubulin, anti-Golgin97 (clone CDF4) (Life Technologies), anti-TMEM87A (clone #772807) (R&D systems), rabbit monoclonal anti-LAMP1 (clone D2D11) (Cell Signaling Technology), rabbit polyclonal anti-VPS53, VPS52 (kindly gifted from Drs. C. Schindler and J. S. Bonifacino (National Institutes of Health) (Perez-Victoria *et al.*, 2008), anti-GPP130 (Covance) and anti-EEA1 were used. The secondary antibodies were PE-conjugated goat anti-mouse IgG (Biolegend), Alexa Fluor 594-conjugated goat anti-mouse IgG, and Alexa Fluor 647-conjugated goat anti-mouse IgG (Life Technologies). Alexa Fluor 488-conjugated CTxB was purchased from Life Technologies. FITC-conjugated lectins were purchased from J-OIL MILLS.

Plasmid construction

A DNA fragment of VSVGex-FF-mEGFP-GPI (VFG-GPI), which encodes a GPI reporter protein, was amplified from pME-Neo2dH-VSVGex-FF-mEGFP-GPI (Maeda *et al.*, 2008). The amplified fragment was cloned into the *Not*I and *Mlu*I sites of pRetroX-Tight-Pur (Clontech) using the In-fusion cloning reagents (Takara) to generate pRetroX-VFG-GPI-Pur. A DNA fragment of Flag-VSVG^{full}-EGFP (FVG-TM), encoding a transmembrane reporter protein, was amplified from pME-FLAG-VSVG^{full}-EGFP (Maeda *et al.*, 2008). The amplified fragment was cloned into pRetroX-Tight-Pur using the same method as used to generate pRetroX-FVG-TM-Pur. A retroviral gene-trap vector containing an adenoviral splice

acceptor (SA) site, a PGK polyA signal, a PGK promoter (PGKpro), the blasticidin-S deaminase (BSD) gene, and human growth hormone (hGH) polyA was constructed as follows. The adenoviral SA site and hGH polyA sequence were amplified from pCMT-SAhygpA-NP21 (Genbank: AB609713) (Horie *et al.*, 2011), which was kindly provided by Dr. Kyoji Horie (Nara Medical University). The primers (SA site) GTTCCTATTCTCTAGAAAGTATAGGAACTTCAGTG and ttGCGGCCGCTCAggTCAgTCAGAATTCCGGCGGCTAGCGATACCGTC, and (hGH polyA) ccTGAGCGGCCGCaaaaATCGATtCTGTGCCTTCTAGTTGCCAGC and TGGACCATCCTCTAGACTGCC were used in the amplification. The amplified fragments were cloned into pCMT-SAhygpA-NP21 at the two *Xba*I sites using the In-fusion cloning reagents, generating pCMT-SA. The PGK polyA and PGKpro sequences were amplified from pCMT-SAhygpA-NP21 using primers CTGACCTGAGCGGCCGCAGAAATTGATGATCTATTAAACAATAAAGA and ggtggACGCGTAGGTCGAAAGGCCCGGAGAT. The BSD gene was amplified from pLIB2-pgkBSD (Maeda *et al.*, 2008) using primers acctACGCGTccaccATGCCTTTGTCTCAAGAAGAATC and GAAGGCACAGAATCGATTTAGCCCTCCCACACATAACC. The resulting PGK polyA-PGKpro and BSD fragments were cloned into the *Not*I and *Cla*I sites of pCMT-SA using In-fusion cloning reagents to generate pCMT-SApA-pgkBSD. The CRISPR/Cas9 expression plasmid, pX330 (Cong *et al.*, 2013), was obtained from Addgene and used to generate pX330-hVPS51, -hVPS52, -hVPS53, -hVPS54#1, and -hVPS54#2; targeting sequences (described below) were cloned into pX330 plasmids digested with *Bbs*I. To construct pX330-mEGFP plasmid, a PCR fragment amplified from a template plasmid, pME-$(G4S)_2$-mEGFP, using primers

(gagaGGCCGGCCAaGCtAAgAAaAAgAAaATGACGCGTGGCGGAG and gagaGGCCGGCCTTcTTgGTtGCgGCaGGtCTcTTtccCTTGTACAGCTCGTCCA) was digested with *FseI* and cloned into the same site of pX330 vector. To generate pX330-mEGFP-hTMEM87A, -hTMEM87B#1 and -hTMEM87B#2, targeting sequences (described below) were cloned into pX330-mEGFP digested with *BbsI*. To express the GARP complex subunits, pEF6-BSD-VPS51, VPS52, VPS53, and mVPS54-V5-6His were kindly gifted by Drs. Juan Bonifacino and Chris Schindler (Perez-Victoria *et al.*, 2008; Perez-Victoria *et al.*, 2010b). To construct the corresponding expression plasmids, VAMP2, VAMP3, VAMP4, VAMP7, STX1A, and STX6 were PCR-amplified from a human brain cDNA library, and GPR107 and GPR108 from HeLa and Hep3B cell cDNA libraries, respectively. The products were cloned into pME-Zeo plasmid digested with *Eco*RI and *Not*I. TMEM87A and TMEM87B cDNAs were amplified from HeLa and Hep3B cell cDNA libraries, respectively, and inserted into pME-Zeo. To construct the N-terminally HA-tagged expression plasmids, TMEM87A and TMEM87B, except for their signal sequences (ss), were PCR-amplified and the *Xho*I- and *Not*I-digested products cloned into pME-ssHA plasmid, which harbors an ss derived from human CD59 upstream of the HA tag. To construct C-terminally 3×HA-tagged expression plasmids, TMEM87A and TMEM87B, except for their stop codons, were PCR-amplified and the products were cloned into *Xho*I- and *Mlu*I-digested pME-3xHA plasmid. To construct pLIB-BSD-VAMP4, pME-Zeo-VAMP4 was digested with *Eco*RI and *Not*I and cloned into pLIB-BSD digested with the same enzymes. Plasmid pLIB-BSD-ssHA-TMEM87A was constructed by PCR-amplifying a cDNA of ssHA-tagged TMEM87A, followed by digestion with *Sal*I and *Not*I and cloning into pLIB2-BSD. To construct

pLIB-Hyg-RFP(S158T)-GPP34, pME-RFP(S158T)-GPP34 was digested with *Eco*RI and *Not*I and cloned into pLIB-Hyg.

Establishment of HAP1FF9, HEK293FF6 and HEK293TM10 cells

Retroviruses were produced in PLAT-GP packaging cells by cotransfection of the VSVG plasmid (pLC-VSVG) and pRetroX-Tet-On Advanced (Clontech) with pRetroX-VFG-GPI-Pur or pRetroX-FVG-TM-Pur. HAP1FF9 cells were established from HAP1 cells, kindly provided by Dr. Thijn R. Brummelkamp (Netherlands Cancer Institute) (Carette *et al.*, 2011b). HAP1 cells were infected with retroviruses bearing pRetroX-VFG-GPI-Pur and pRetroX-Tet-On Advanced, followed by selection with puromycin and G418. A HAP1FF9 cell clone was obtained after limiting dilution and karyotype analysis.

HEK293FF6 and HEK293TM10 cells were established from HEK293 cells by infection with retroviruses bearing pRetroX-Tet-On Advanced and pRetroX-VFG-GPI-Pur or pRetroX-FVG-TM-Pur, respectively, followed by selection with puromycin and G418, and limiting dilution.

Cell culture

HAP1FF9 cells were cultured in Iscove's Modified Dulbecco's Medium (IMDM) supplemented with 10% FCS, 600 μg/ml G418 and 6 μg/ml puromycin. HEK293FF6, HEK293TM10, GARP-KO cell lines, and TMEM87A and B double-KO (DKO) cell line established from HEK293FF6, were cultured in DMEM supplemented with 10% FCS, 600 μg/ml G418 and 1 μg/ml puromycin. V54KO cells stably expressing either empty vector, mVPS54-V5-His, hVAMP4, or ssHA-hTMEM87A (V54KO+Vec, V54KO+VPS54, V54KO+VAMP4, and V54KO+TM87A, respectively) were cultured in DMEM supplemented with 10% FCS, 600 μg/ml G418, 1 μg/ml puromycin and 10

μg/ml blasticidin. V54KO+Vec and V54KO+VPS54 stably expressing RFP(S158T)-GPP34 were cultured in DMEM supplemented with 10% FCS, 600 μg/ml G418, 1 μg/ml puromycin, 10 μg/ml blasticidin, and 500 μg/ml hygromycin B. RFP(S158T)-GPP34, a fusion protein of enhanced RFP and TGN protein GPP34, is used as a TGN marker (Shaner *et al.*, 2008).

Enrichment of transport-delayed HAP1FF9 mutant cells

A gene-trap virus was produced by transfection of PLAT-GP cells in eight 15-cm dishes using Lipofectamine 2000 and a mixture of pCMT-SApA-BSD and pLC-VSVG. The virus-containing supernatant was concentrated five times using PEG-it solution and then mixed with 8 μg/ml polybrene. HAP1FF9 cells (6×10^7 cells in total) prepared in 6-well plates containing 2.5×10^6 cells per well were infected by centrifugation at 2,500 rpm for 2 h at 32°C. Two days after infection, the cells were selected with 6 μg/ml blasticidin for 1 week. HAP1FF9 cells mutagenized by gene-trap vectors were cultured in medium containing 1 μg/ml Dox at 40°C for 24 h to induce and accumulate the VFG-GPI reporter protein in the ER (Maeda *et al.*, 2008; Fujita *et al.*, 2009). The cells were then quickly harvested with trypsin-EDTA and incubated in medium at 32°C for 60 min, followed by staining with an M2 anti-Flag antibody and PE-conjugated goat anti-mouse IgG. Cells with decreased surface expression of the reporter protein were enriched twice by cell sorting using a FACSAria (BD Bioscience).

Sequence analysis of the gene-trap insertion sites

Genomic DNA was isolated from 3×10^7 cells using the Wizard Genomic DNA purification kit (Promega) according to the manufacturer's protocol. Genomic DNA (15 μg) was digested with *Hae*III, followed by ligation with the splinkerette adaptor (Horie *et al.*, 2011), which consists of two oligonucleotides: Spl-top-HaeIII

(CGAATCGTAACCGTTCGTACGAGAATTCGTACGAGAATCGCTGTCCTCTCC AACGAGCCAAGG) and SplB-BLT-HaeIII (CCTTGGCTCGTTTTTTTTTGCAAAAA). After ligation, the DNA fragments were digested with *Pvu*II, which cleaves the vector sequence between the 3′LTR and the upstream *Hae*III site, to prevent unwanted vector amplification. After column purification, the fragments were used as templates for splinkerette PCR using the SPl-P1 primer (CGAATCGTAACCGTTCGTACGAGAA) and the first LTR primer (AGTGTATGTAAACTTCTGACCCACTGG). The resulting DNA fragments were further amplified by nested PCRs using the SPl-P2 primer (TCGTACGAGAATCGCTGTCCTCTCC) and the second LTR primer (CTTGTGTCATGCACAAAGTAGATGTCC) for the first PCR, Rd1Tru-LTR (ACACTCTTTCCCTACACGACGCTCTTCCGATCTGCTAGCTTGCCAAACCTAC AGGTGGG), and Rd2Tru-Splink (GTGACTGGAGTTCAGACGTGTGCTCTTCCGATCTGCTGTCCTCTCCAACGAG CCAAGG) for the second PCR. The underlined sequences indicate the Illumina sequencing primers. The resulting DNA products contained the end of the 5′LTR retroviral sequence followed by the genomic DNA sequence flanking the insertion site ending at the *Hae*III restriction site and part of the splinkerette adaptor sequence. Illumina P5 (AATGATACGGCGACCACCG) and P7 (CAAGCAGAAGACGGCATACGA) adapters and barcode sequences were attached to the products by 6 cycles of PCR with 10 ng of each of initial PCR product as the template. Paired-end sequencing (151-bp × 2) was performed on the MiSeq (Illumina) system. The numbers of reads obtained from control cells and Sort 2 cells were approximately 1.4 million and 1.2 million, respectively.

Analysis of gene-trap insertions

FASTQ data files were analyzed using CLC Genomic Workbench software version 7.0.4 (CLC bio) according to a previously described method (Carette *et al.*, 2011a; Carette *et al.*, 2011b). Briefly, after quality trimming and removal of the common LTR sequence, the 50-bp reads were mapped onto the human genome (hg19). To exclude ambiguous alignments, mismatch reads were not allowed and all non-specific matched reads were ignored. To eliminate PCR amplification bias and to determine the unique insertion sites, duplicate reads were removed and counted as one read (a unique insertion site). The independent insertion sites were further classified as being in the sense or antisense orientation compared to the gene. The total number of inactivating insertions, which consisted of all the sense or antisense orientations in the exons of the genes and the number of inactivating insertions per individual gene, were counted. The amount of enrichment of a particular gene in the screen was calculated by comparing the selected with the unselected population. For each gene, a *P*-value and a *P*-value corrected for the false-discovery rate (FDR) were calculated by the one-sided Fisher exact test using the R software. A bubble plot was created using R software.

Establishment of knockout cell lines

GARP-KO cell lines and TM87A, B-DKO cell lines were generated using the CRISPR-Cas9 system. For the generation of GARP-KO cell lines, HEK293FF6 cells were transiently transfected with pX330 plasmids bearing the targeting sequence for VPS51 (GGGAGGCTCCGGAGCGTCGG), VPS52 (GGCCCGGGAACTGGTGTTGC), VPS53 (GCTCACGCCCGAGGTGCAGC) and VPS54 (#1; GAGGCACTGGTGAAGAACTG and #2; GGACACACATCTGGCAGTGA). After about 10 days of culture, cells with delayed

VFG-GPI transport were sorted using a FACS-Aria cell sorter. The collected population was subjected to limiting dilution. To generate TM87A, B-DKO cell lines, HEK293FF6 cells were transiently transfected with pX330-mEGFP plasmids bearing the targeting sequence for hTMEM87A (GGAACAAACCTTACCTTTAT). After 3 days, cells with EGFP were sorted using a FACS-Aria cell sorter. The collected cells were subjected to limiting dilution. A clone, which had no wild-type allele, was picked up and used for next round knock out process. A TMEM87A KO cell line was transiently transfected with pX330-mEGFP plasmids bearing the either targeting sequence for hTMEM87B#1 or #2 (#1; GCCGCCGCTGCTTTCCCGCC, #2; GACCCCGGCGGCTGTGCGCG). After cell sorting, collected cells were subjected to limiting dilution. DNA sequences were analyzed by the Sanger method. The DNA sequence of each KO cell line was listed in Table.

Transport assay of reporter proteins using FACS

The transport assay was conducted as previously described (Maeda *et al.*, 2008; Fujita *et al.*, 2009). Briefly, cells were cultured in medium supplemented with 1 μg/ml Dox at 40°C for 24 h, harvested using trypsin-EDTA (Sigma), and then incubated in complete medium at 32°C for the required time. The cells were stained with an M2 anti-FLAG antibody and PE-conjugated goat anti-mouse IgG and then analyzed by FACS-CantoII (BD). For the KD experiments, 0.5×10^6 cells were transfected with siRNA oligonucleotides purchased from Life Technologies using the lipofectamine RNAi MAX reagent. Two days later, the cells were retransfected with the same siRNA oligos. On the following day, they were cultured in complete medium supplemented with 1 μg/ml Dox at 40°C for 24 h, after which transport was analyzed as described above. The siRNA sequences used were as follows: STX6#1:

(GCAACUGAAUUGAGUAUAATT, siRNA ID: s19959); STX6#2: (GCAGUUAUGUUGGAAGAUUTT, siRNA ID: s19960); VAMP4#1: (CAAACAACUUCGAAGGCAATT, siRNA ID: s16525); VAMP4#2: (GAUUUGGACCUAGAAAUGATT, siRNA ID: s16526). For the transient expression of FVG-TM, 0.5×10^6 cells were transfected with pME-FLAG-VSVG^{full}-EGFP using the Lipofectamine 2000 reagent. On the following day, the incubation temperature was shifted to 40°C for 48 h. If required, expression plasmids alone or together with pME-FLAG-VSVG^{full}-EGFP, were transfected into the cells described above.

Western blotting

Cell lysate was prepared by incubation in buffer containing 50 mM Tris-HCl (pH7.4), 150 mM NaCl, 1% Triton X-100, 5 mM EDTA and 1× protease inhibitor cocktail (Roche), followed by centrifugation at 15,000 rpm for 15 min. Supernatant was recovered, mixed with SDS sample buffer and boiled at 95 °C for 5 min. Samples were run on 10-20% SDS-PAGE gels and transferred to PVDF membranes. VPS52, VPS53, GAPDH, STX6 and α-tubulin were detected by anti-VPS52, anti-VPS53, anti-GAPDH, anti-STX6 and anti-α-tubulin antibodies.

Quantitative reverse-transcription PCR (qRT-PCR)

Total RNA was prepared using RNeasy mini kit (QIAGEN) and was used for generating cDNA by SuperScript VILO cDNA synthesis kit (LifeTechnologies). qRT-PCR was performed using SYBR Premix Ex Taq II (Tli RNase H plus) purchased from TaKaRa. The RNA expression was normalized by HPRT1 expression and the relative expression was calculated by $\Delta\Delta C_T$ method.

Immunofluorescence microscopy

The cells were fixed with PBS containing 4% PFA for 20 min at room

temperature, followed by washing with 40 mM NH_4Cl for 10 min. The cells were double-stained with anti-TMEM87A or anti-HA7 and anti-GPP130 antibody as the primary antibodies dissolved in staining buffer A1 (PBS containing 2.5% goat serum, 0.1% NaN_3, and 0.1% Triton X-100) followed by Alexa488-conjugated goat anti-mouse IgG and Alexa594-conjugated goat anti-rabbit IgG as the secondary antibodies in staining buffer A2 (PBS containing 1% BSA, 0.1% NaN_3, and 0.1% Triton X-100). For intracellular localization of CD59, cells were pre-treated with 1 unit/ml PI-PLC (Life Technologies) for 1.5 h at 37°C. The cells were double-stained with anti-CD59 and anti-LAMP1 or anti-EEA1 dissolved in staining buffer B1 (PBS containing 2.5% goat serum, 0.1% NaN_3, and 0.1% saponin) followed by the secondary antibodies as described above in staining buffer B2 (PBS containing 1% BSA, 0.1% NaN_3, and 0.1% saponin). Confocal images were acquired on a FluoView FV1000 (Olympus).

Flow cytometric analysis

Cells were stained with anti-CD59 in FACS buffer (PBS containing 1% BSA, 0.1% NaN_3) followed by staining with PE-conjugated goat anti-mouse IgG in FACS buffer. Surface glycosylation profiles were analyzed by FITC-conjugated lectins in FACS buffer containing 1 mM $CaCl_2$, 1 mM $MnCl_2$, and 1 mM $MgCl_2$.

Transport assay of reporter proteins based on immunofluorescence microscopy analysis

Cells stably expressing RFP(S158T)-GPP34 were cultured in medium supplemented with 1 μg/ml Dox at 40°C for 24 h. On the following day, they were washed with cold PBS and chased with warmed complete medium at 32°C containing 100 μg/ml cycloheximide (CHX) for the indicated time followed by fixation. For post-Golgi anterograde transport analysis, the cells were pre-cultured at 19°C for 3 h with complete medium containing 100 μg/ml CHX and then chased at 32°C. After

fixation, the cells were stained with M2 anti-FLAG antibody and Alexa647-conjugated goat anti-mouse IgG; the antibodies were dissolved in staining buffer without detergent. Images were obtained as described above.

Retrograde transport assay of CTxB

The cells were washed twice with PBS and then cultured in cold medium supplemented with 10 mM HEPES and 1 μg/ml Alexa488-conjugated CTxB for 30 min on ice. After incubation, the cells were washed with ice cold PBS once and incubated in warmed complete medium at 37°C for indicated time, followed by fixation and staining with combinations of anti-Golgin97 antibody dissolved in staining buffer A1 and Alexa594-conjugated goat anti-mouse IgG dissolved in staining buffer A2. Images were obtained as described above.

Quantification of immunofluorescence images

Fluorescence intensities were quantified using MetaMorph 3.0 (Molecular Devices). The VFG-GPI, CD59 or CTxB regions and the TGN (RFP-GPP34- or Golgin-97-positive regions), cell surface (FLAG positive regions) or lysosomes (LAMP1 positive regions) in each fluorescence image were assigned a threshold by MetaMorph 3.0. The fluorescence intensities of total VFG-GPI, CD59 or CTxB ($I_{(t)}$) and VFG-GPI, CD59 or CTxB that colocalized with markers ($I_{(m)}$) were measured and their ratios were expressed as the percentage of $I_{(m)}$ in $I_{(t)}$. Means and standard errors were calculated and plotted from 10 independent fluorescence images.

Expression cloning

A retroviral-based cDNA library from human brain was stably transfected into V54KO cells. Those cells with increased transport rate were sorted using a cell sorter. The culture and sorting steps were repeated once more. Genomic DNA was isolated

from pre-enrichment control cells and the sorted cells as described above. Genomic DNA (15 μg) was digested with Covaris S2 (M&S) using the 800-bp protocol, followed by repair of the ends of the products and ligation with the above-mentioned splinkerette adaptor. After ligation, the DNA fragments were used as templates for splinkerette PCR using the primers SPl-P2 and pLIB-F0 (CTCCCTTTATCCAGCCCTCACTCC). The resulting DNA fragments were further amplified by PCR using Rd1Tru-pLIB (ACACTCTTTCCCTACACGACGCTCTTCCGATCTCGCCGGAATTCGTTAGGCC ATTA) and Rd2Tru-Splink (GTGACTGGAGTTCAGACGTGTGCTCTTCCGATCTGCTGTCCTCTCCAACGAG CCAAGG). The underlined sequences indicate the Illumina sequencing primers. Illumina P5 and P7 adapters and barcode sequences were attached as described above and single-end sequencing (151-bp) was performed on the HiSeq2500 (Illumina) system. The numbers of reads obtained from control and the sorted cells were approximately 26 million and 7.2 million, respectively.

Sequence analysis of recovered cDNAs

FASTQ data files were analyzed using CLC Genomic Workbench software version 7.0.4. After quality trimming and removal of the common pLIB sequence, the reads were mapped to the human genome (hg19). For each gene, test statistics, a *P*-value, and the *P*-value corrected for the FDR of Kal's Z-test were calculated by comparing the number of mapped reads using CLC Genomic Workbench software version 7.0.4 (Kal *et al.*, 1999).

6. Results

Screening mutant haploid cells defective in GPI-AP transport

To identify genes necessary for the efficient anterograde transport of GPI-APs, I took advantage of forward genetic screening in human haploid cells, HAP1 cells (Carette *et al.*, 2011b). Because gene function can be easily destroyed by one hit mutation in haploid cells, forward genetic screening can be applied to HAP1 cells. To monitor the anterograde transport of GPI-AP, a GPI-anchored reporter protein which was previously developed in genetic screening with CHO cells was used (Maeda *et al.*, 2008; Fujita *et al.*, 2009). This reporter is a chimeric protein consisting of a luminal domain of $VSVG^{ts}$, a FLAG tag, an EGFP, and a C-terminal GPI attachment signal (VFG-GPI). $VSVG^{ts}$ causes accumulation of the reporter in the ER at the restrictive temperature of 40°C, because of the unfolding status of $VSVG^{ts}$. In contrast, $VSVG^{ts}$ can be rapidly folded at the permissive temperature of 32°C, which allows us to start transport of proteins synchronously. Therefore, transport status at *x* min after the temperature shift can be estimated by the ratio of surface arrived proteins (staining with anti-FLAG antibody under non-permeabilized conditions) to total one (fluorescence of EGFP) using flowcytometry. Thus, I first established a HAP1 cell line, HAP1FF9, with doxycycline (Dox)-inducible expression of VFG-GPI and mutagenized the cells using a retroviral gene-trapping vector. Control genomic DNA was extracted before the enrichment of transport mutants. Using a cell sorter, mutant cells showing slow GPI-AP transport, as determined by decreased surface levels of VFG-GPI, were collected 60 min after the temperature shift. The collected cells were cultured and then resorted to enrich mutants with delayed GPI-AP transport (Sort 2, Fig. 2A). Retroviral insertion sites in the genomic DNA from Sort 2 cells and control pre-enrichment cells were

analyzed by deep sequencing. Enrichment rates were calculated for the respective genes by comparing the numbers of mapped independent-insertion sites of the respective gene between Sort 2 and control cells. The genes *PGAP1* and *PGAP5* (*MPPE1*), whose mutations have been known to cause delayed transport of GPI-APs, were enriched in Sort 2 (Fig. 2B), indicating the usefulness of the method. In addition, *PGAP2* gene, which is required for the GPI fatty acid remodeling in the Golgi (Tashima *et al.*, 2006), was also enriched in Sort 2. In the *PGAP2* mutant cells, transport of GPI-APs is almost normal, but the surface expression of GPI-APs is greatly decreased because lyso form GPI-APs, the intermediate form during the fatty acid remodeling which harbors only single acyl-chain, are not reacylated due to PGAP2 defect and are released easily from the membrane into medium soon after arrival at the cell surface.

Knockout of GARP complex subunits severely impairs anterograde transport of proteins

Three genes, *C11orf2* (also known as *VPS51* or *Ang2*), *VPS52,* and *VPS54*, encoding subunits of the GARP complex, a tethering factor involved in endosome-to-TGN retrograde transport, were significantly enriched in Sort 2 cells ($p<0.01$) and the fourth subunit VPS53 was positioned close to the significance limit (Fig. 2B). In addition, *COG8* gene encoding a subunit of conserved oligomeric Golgi (COG) complex, another multi-subunit tethering factor and involved in endosome-to-TGN retrograde transport, was highly enriched, suggesting endosome-to-TGN retrograde transport might be important for the anterograde transport of GPI-APs. To investigate whether the GARP complex is involved in the anterograde transport of GPI-APs, I generated GARP-KO cells using the CRISPR-Cas9 system (Cong *et al.*, 2013; Mali *et al.*, 2013) in HEK293FF6 cells, bearing Dox-inducible

VFG-GPI. All mutations caused frame-shifts (Table), indicating that all mutant cells had completely lost expression of the targeted genes. Indeed, VPS52 and VPS53 proteins were nearly completely disappeared in V52KO and V53KO cells, respectively (Fig. 3A). To compare the kinetics of anterograde transport of VFG-GPI, I conducted a transport assay using HEK293FF6 wild-type or GARP-KO cells. The relative expression of VFG-GPI in each KO cell line (V51KO, V52KO, V53KO, and V54KO) 90 min after the temperature shift was 14.7 ± 5.2%, 21.7 ± 11.0%, 5.9 ± 1.7%, and 27.0 ± 3.5%, respectively (mean ± SD, Figs. 3B and C), suggesting that the anterograde transport of GPI-APs is severely impaired in GARP-KO cells. To investigate whether delayed transport was specific to GPI-APs, I conducted a similar transport assay of a transmembrane type reporter protein in GARP-KO cells. The reporter protein, FVG-TM, was a chimeric protein consisting of a FLAG tag, $VSVG^{ts}$ (full length), and EGFP (Maeda *et al.*, 2008; Fujita *et al.*, 2009). Because HEK293FF6 cell line does not have FVG-TM, its expression plasmid was transiently transfected into cells and its transport then assayed. After 90 min, the relative expression of FVG-TM in V51KO, V52KO, V53KO, and V54KO cells was only 3.7 ± 0.95%, 8.0 ± 2.5%, 2.4 ± 1.3%, and 18.6 ± 7.0%, respectively (mean ± SD, Figs. 3D and E). Expression of the responsible gene in each KO cell restored the delayed transport of both VFG-GPI and FVG-TM (Fig. 3F), thus ruling out off-target effects. These results indicated that the GARP complex is required for the efficient anterograde transport of both GPI-anchored and transmembrane proteins.

Post-Golgi anterograde transport is defective in V54KO cells

To analyze which step of the transport is impaired in GARP KO cells, I performed

the transport assay using confocal microscopy in cells stably transfected with an empty vector or VPS54 (V54KO+Vec or V54KO+VPS54), together with RFP-GPP34 as a TGN marker. VFG-GPI was accumulated in the ER, followed by transport for indicated time after which the cells were fixed to terminate the transport. Ratios of VFG-GPI fluorescence intensity in the TGN to total cellular VFG-GPI fluorescence intensity were determined at each time point (Fig. 4B). In V54KO+VPS54 cells, the amount of VFG-GPI that reached the TGN increased for 20 min and gradually decreased at 90 min (Figs. 4A and B), suggesting that after VFG-GPI reached the TGN it was transported to the cell surface. In V54KO+Vec cells, the relative intensity in TGN was slightly increased at 20 min but it further increased for the next 60 min (Figs. 4A and B), suggesting that after its arrival at the TGN, VFG-GPI accumulated in the TGN for at least 60 min. This result suggested that KO of VPS54 causes impairment of post-Golgi transport. Although ER-to-Golgi transport appeared to be slightly affected in V54KO+Vec cells (0.15 ± 0.012 vs. 0.095 ± 0.0089 at 20 min; mean ± SEM), this might have been because of the indirect effect of delayed post-Golgi transport. To confirm that post-Golgi anterograde transport is impaired in V54KO cells, I analyzed the post-Golgi anterograde transport directly. It is known that post-Golgi anterograde transport can be reversibly arrested at 19°C (Matlin and Simons, 1983). After VFG-GPI was accumulate in the Golgi at 19°C, transport was chased for 45 min and VFG-GPI that reached cell surface was stained with anti-FLAG antibody under non-permeabilized conditions. Ratios of VFG-GPI fluorescence intensity in the cell surface to total cellular VFG-GPI fluorescence intensity were quantified (Fig. 4D). As shown in Fig. 4C, at 0 min most of the VFG-GPI were localized in the TGN in both V54KO+VPS54 and V54KO+Vec cells. By 45 min, although a large amount of the VFG-GPI reached the

cell surface in V54KO+VPS54 cells (Figs. 4C and D), this was barely the case in V54KO+Vec cells, as VFG-GPI largely remained in the TGN (Figs. 4C and D). This result strongly pointed out the requirement of the GARP complex in post-Golgi anterograde transport.

CD59, an endogenous GPI-AP, was missorted to lysosomes in V54KO cells

The fact that post-Golgi anterograde transport was impaired in V54KO cells led me to investigate whether the cargo sorting at the TGN was impaired. To elucidate this point, intracellular localization of endogenous GPI-AP, CD59, was analyzed. To eliminate cell surface CD59, cells were treated with phosphatidylinositol-specific phospholipase C (PI-PLC) before fixation and analyzed by confocal microscopy because GPI-APs were specifically released from cell surface by PI-PLC. In V54KO+VPS54 cells, intracellular CD59 was hardly detectable whereas many CD59 positive vesicles were observed in V54KO+Vec cells (Fig. 5A). These vesicles were largely colocalized with LAMP1, but not with EEA1 (Figs. 5A and B). This result suggested that CD59 was missorted to lysosomes in V54KO cells probably due to defective post-Golgi anterograde transport. If most of GPI-APs are missorted to lysosomes and degraded, it is possible that surface expression of GPI-APs is reduced. However, flow cytometric analysis revealed that surface expression of CD59 was not reduced in V54KO+Vec cells compared to V54KO+VPS54 cells (Fig. 5C), suggesting that the majority of GPI-APs are properly but slowly transported to the cell surface.

GARP-KO caused abnormal O-glycosylation but not N-glycosylation

Previous studies indicated that defective vesicular transport disrupted protein

glycosylation (Wu *et al.*, 2004; Ong *et al.*, 2014). Some congenital disorders of glycosylation are caused by the mutations in the subunits of COG complex (Wu *et al.*, 2004; Climer *et al.*, 2015). Thus, I postulated that GARP deficiency might cause the abnormal glycosylation. To investigate this, I analyzed the surface glycosylation profile by fluorescent labeled lectins. The staining patterns of Con A, WGA, LCA, and MAM, all of them specifically bound to N-glycosylation, were not altered in V54KO+Vec cells (Fig. 6A), suggesting that GARP complex was not indispensable to N-glycosylation. In contrast, V54KO+Vec cells showed higher staining with SBA or PNA, and lower staining with UEA-I, all of them bound to O-glycosylation (Fig. 6A). As SBA or PNA bind to desialylated form of O-glycans, these results indicated the decreased sialylation efficiency in V54KO cells. The epitope of UEA-I is fucose linked to O-glycan, suggesting lower levels of fucosylation on O-glycans in V54KO cells. These results implied that GARP-KO specifically affected O-glycosylation but not N-glycosylation. To further examine this, I performed western blotting analysis. The molecular weight of TfR containing N-glycosylation only was not altered in V54KO+Vec or V53KO+Vec cell (Fig. 6B). In contrast, some of DAF or LAMP1 in V54KO+Vec or V53KO+Vec cells ran faster, both of them contained O-glycosylation (Fig. 6B). These results supported the notion that GARP complex is required for collect O-glycosylation but not N-glycosylation. To get an insight for surface glycolipid profile, I used bacterial toxin, cholera toxin B subunit (CTxB), which bound to GM1. The staining with CTxB was also decreased in V54KO+Vec cells (Fig. 6A), indicating lower surface expression of GM1. To investigate the intracellular localization of GM1, I stained GM1 with CTxB under pearmebilized conditions and analyzed by confocal microscopy. Most of GM1 was localized in plasma membrane in V54KO+VPS54 cells whereas smaller amount of

GM1 was observed in plasma membrane but instead many intracellular pools were detectable in V54KO+Vec cells (Fig. 6C). These results indicated that GARP complex is involved in GM1 localization.

VAMP4-mediated retrograde transport is required for recycling of proteins critical for efficient anterograde transport

The GARP complex tethers endosome-derived transport carriers to the TGN, so endosome-to-TGN retrograde transport may contribute to post-Golgi anterograde transport by recycling the molecules involved. Thus, in V54KO cells less of these molecules, such as SNARE proteins, would be found in their expected location. If this is true, overexpression of SNAREs may restore the defective anterograde tansport in V54KO cells. To examine this possibility, several SNARE proteins localized in the post-Golgi compartments were overexpressed in V54KO cells and restoration of anterograde transport was then assessed. Overexpression of VAMP4 partially restored the delayed transport of both VFG-GPI and FVG-TM whereas overexpression of VAMP2, VAMP3, VAMP7, STX1A, or STX6 did not (Fig. 7). Because VAMP4 is involved in the endosome-to-TGN retrograde transport, I predicted to restore the defective endosome-to-TGN retrograde transport in V54KO cells. To investigate this possibility, I analyzed plasma membrane to TGN retrograde transport using CTxB as a cargo. I prepared V54KO cells stably expressing VAMP4 (V54KO+VAMP4) and collected cells that restored anterograde transport of VFG-GPI (Fig. 8A). To assess CTxB retrograde transport, Alexa488-conjugated CTxB was bound to the cell surface at 4°C, after which cells were incubated at 37°C for 60 min to allow the transport of CTxB. Because CTxB binding to the cell surface was decreased in V54KO cells as described

above (Fig. 6A), retrograde transport efficiency was determined by comparing the ratio of Golgi-localized CTxB to total CTxB. The ratio of CTxB localized in the TGN at 60 min in V54KO+Vec cells was lower than that in V54KO+VPS54 cells (Figs. 8B and C), indicating the impairment of endosome-to-TGN retrograde transport in V54KO cells, consistent with the findings of a previous study (Perez-Victoria *et al.*, 2008). As shown in Figs.8B and C, the amount of TGN-localized CTxB at 60 min was clearly higher in V54KO+VAMP4 cells than in V54KO+Vec cells (0.21 ± 0.024 vs. 0.15 ± 0.016; mean ± SEM). I interpreted this data that retrograde transport of CTxB was partially restored by VAMP4 overexpression and that the statistic insignificance (p=0.055) may be accounted for by the presence in V54KO+VAMP4 cells of a population that did not restore the anterograde transport (Fig. 8A). These results and those on the restoration of anterograde transport strongly indicated that VAMP4-mediated retrograde transport is important for the recycling of molecules involved in the anterograde transport of both GPI-anchored and transmembrane proteins. This conclusion was confirmed by using siRNA to abolish the expression of VAMP4 or STX6. For this experiment, we used a HEK293FF6 cell line for VFG-GPI transport and a HEK293TM10 cell line, in which expression of FVG-TM could be induced with Dox. As shown in Fig. 8D, both STX6 and VAMP4 expression were efficiently knocked down. Depletion of VAMP4 or STX6 impaired the anterograde transport of both VFG-GPI and FVG-TM (Fig. 8E). These results were consistent with the result from the VAMP4 overexpression experiments. These results supported an idea that post-Golgi anterograde transport was coupled with GARP- or VAMP4-dependent endosome-to-TGN retrograde transport.

Potential role for TMEM87A and TMEM87B in endosome-to-TGN retrograde transport

In other words, some molecules required for the post-Golgi anterograde transport should be recycled back to the TGN in a GARP dependent manner. To identify such molecules, I performed the screening of genes whose overexpression can restore the delayed transport inV54KO cells. This is based on the idea that overproducing of the molecules can compensate the lack of molecules in the TGN in V54KO cells. A cDNA library derived from human brain was introduced into V54KO cells, and the cDNAs in the transport-restored cell populations were sequenced by next generation sequencer. From this screening, *TMEM87A*, encoding a multi-pass transmembrane protein belonging to the LU7TM family (from Uniprot), was obtained. Overexpression of TMEM87A partially restored the defect in anterograde transport of both VFG-GPI and FVG-TM in V54KO cells (Fig. 9A: Geometric means of cell surface levels of VFG-GPI and FVG-TM were 1.92±0.22 and 4.45±1.1 times, respectively, of those in V54KO+Vec (n=3)). Overexpression of TMEM87B, a close homolog of TMEM87A and a member of the same family, also restored the defect in V54KO cells (Fig. 9A: Geometric means of cell surface levels of VFG-GPI and FVG-TM were 1.85±0.22 and 3.42±0.99 times, respectively, of those in V54KO+Vec (n=3)), suggesting its functional redundancy with TMEM87A. Recently, a role for GPR107—another LU7TM family member—was shown to be retrograde transport of toxins such as exotoxin A of *Pseudomonas aeruginosa* and ricin (Carette *et al.*, 2011a; Elling *et al.*, 2011; Tafesse *et al.*, 2014; Zhou *et al.*, 2014). Unlike TMEM87A and TMEM87B, overexpression of GPR107 or GPR108, a member of LU7TM family closely related to GPR107, did not restore the delayed transport of either VFG-GPI or FVG-TM in V54KO cells (Fig. 9B: Geometric means of cell surface levels of VFG-GPI and FVG-TM in V54KO+GPR107 were 1.21±0.38 and 0.98±0.11 times, respectively, of those in V54KO+Vec (n=2); and

those in V54KO+GPR108 were 1.23±0.14 and 1.15±0.027 times, respectively, of those in V54KO+Vec (n=2)). These results suggested the specific function of TMEM87A and TMEM87B. Because these two proteins have not been characterized, I first investigated their localization in mammalian cells. Because endogenous TMEM87A protein could not be detected by immunoblotting and immunofluorescence analysis in HEK293 cells, expression plasmids of N-terminally HA-tagged or C-terminally 3×HA-tagged TMEM87A and TMEM87B were constructed and their functions were confirmed based on their ability to restore the V54KO phenotype. Overexpression of N- or C-terminally tagged TMEM87A restored the impairment of anterograde transport of VFG-GPI to an extent similar to that of the non-tagged version (data not shown), indicating that both HA-tagged TMEM87As were functional; by contrast, neither of the tagged TMEM87Bs were functional. Non-tagged or N- or C-terminally HA-tagged TMEM87A was transiently expressed in wild-type cells and the localization of the proteins was analyzed by confocal microscopy. As shown in Fig. 9C, non-tagged or N- or C-terminally HA-tagged TMEM87A predominantly colocalized with GPP130, indicating its Golgi localization.

Because overexpression of TMEM87A or TMEM87B could restore the impaired anterograde transport of both GPI-anchored and transmembrane proteins, these proteins may not be specific cargo receptors for GPI-APs. So, I assumed that the mechanisms by which TMEM87A overexpression restored anterograde transport in V54KO cells was overcoming the impaired retrograde transport. To investigate this, I examined the retrograde transport of CTxB in TMEM87A-overexpressing cells. Thus, N-terminally HA-tagged TMEM87A was stably expressed in V54KO cells (V54KO+TM87A) and cells in which anterograde transport of VFG-GPI was partially restored were collected

(Fig. 9D). At 60 min, TGN-localized CTxB levels were significantly higher in V54KO+TM87A cells than in V54KO+Vec cells (Figs. 9E and F), which indicated that the V54KO phenotype could be restored by the restoration of retrograde transport in V54KO cells. Finally, I investigated whether a loss of TMEM87A and B affects retrograde transport of CTxB. For this, I generated TMEM87A and TMEM87B double-KO (TM87A, B-DKO) cell lines using HEK293 cells. HEK293 cells expressed both genes at levels comparable to VPS51 and VPS54 as assessed by qRT-PCR (Fig. 10A). Contrary to my expectation, retrograde transport of CTxB was not affected in TM87A, B-DKO cell lines (data with clone #2 shown in Fig. 10B). It seemed that TMEM87A and B were not directly involved in retrograde transport of CTxB or that yet another protein is redundantly involved. It is, therefore, likely that overexpression of TMEM87A or B in V54KO cells enhanced retrograde transport efficiency in general. Taken together, our data provide evidence that TMEM87A and TMEM87B are Golgi-localized proteins involved in endosome-to-TGN retrograde transport.

7. Discussion

The aim of this study was to identify genes necessary for the efficient anterograde transport of GPI-APs. Forward genetic screening using human haploid cell line identified genes encoding subunits of the GARP complex. Depletion of each component of this complex revealed its requirement in the anterograde transport of both GPI-anchored and transmembrane proteins. In V54KO cells, post-Golgi anterograde transport was severely delayed, consistent with localization of the GARP complex within the TGN (Perez-Victoria *et al.*, 2008). The delay in anterograde transport in V54KO cells was partially restored by the overexpression of VAMP4, but not VAMP3, which also functions in endosome-to-TGN retrograde transport (Mallard *et al.*, 2002). VAMP4 overexpression also repaired the endosome-to-TGN retrograde transport defect. According to these results, the defective anterograde transport in GARP-KO cells was caused by impaired endosome-to-TGN retrograde transport. Additionally, knockdown of VAMP4 or STX6 resulted in the defective anterograde transport of both GPI-anchored and transmembrane proteins. These results support a model in which endosome-to-TGN retrograde transport mediated by VAMP4 and GARP is required for recycling of molecules critical for post-Golgi anterograde transport (Fig. 11). Although the possibility that the GARP complex is directly involved in anterograde transport cannot be ruled out, this is unlikely because the overexpression of VAMP2, which forms a complex with plasma membrane-localized t-SNAREs and is required for the post-Golgi anterograde transport of proteins (Calakos *et al.*, 1994; Olson *et al.*, 1997; Chen and Scheller, 2001), could not restore delayed anterograde transport in V54KO cells (Fig. 7).

Recently, it has been reported that members of GARP complex form another

protein complex, termed endosome-associated recycling protein (EARP), which is the multi-subunit tethering factor required for endocytic recycling (Schindler *et al.*, 2015). In addition to VPS51, VPS52 and VPS53, EARP complex contains syndetin (also known as CCDC132 or VPS50) instead of VPS54. We produced VPS51, 52, 53, 54 KO cells. In the VPS51, 52 or 53 KO cells, both GARP and EARP functions would be impaired. In this study, however, VPS54 KO cells showed defects in anterograde protein transport from the Golgi, suggesting GARP function itself for tethering of endosome-derived vesicles to the Golgi is important for the transport.

COG8 gene, encoding a subunit of COG complex, was identified in this screening (Fig. 2B). Similar to GARP complex, COG complex is a multi-subunit tethering factor composed of eight subunits (Ungar *et al.*, 2006). COG complex acts as a tethering complex required for intra-Golgi or endosome-to-TGN retrograde transport (Oka *et al.*, 2004; Laufman *et al.*, 2011). Either one of these functions of COG or both might contribute to post-Golgi anterograde transport of integral membrane proteins.

My results indicated that loss of GARP complex disturbed O-glycosylation, especially sialylation or fucosylation, but not N-glycosylation (Figs. 6A and B). It is interesting since specific defect in O-glycosylation has not been reported previously; for instance, loss of COG complex led to abnormal glycosylation of both N-glycosylation and O-glycosylation (Spaapen *et al.*, 2005). Thus, I speculated that some glycosyltransferases for O-glycosylation transiently exited from the post-Golgi compartment and recycled back through endosomes in a GARP dependent manner. To confirm this, further analyses are needed. I also examined the surface expression of GM1 ganglioside and found the low expression of GM1 in V54KO cells (Fig. 6A). In contrast to low expression on cell surface, large amount of GM1 were detected as

intracellular pools in V54KO+Vec cells (Fig. 6C). Recent study suggested that GARP complex is involved in the lipid metabolism especially for sphingolipids and cholesterol (Frohlich *et al.*, 2015). In VPS53 KD cells, cholesterol was highly accumulated in intracellular space (Frohlich *et al.*, 2015) consistent with my observation of GM1 localization in V54KO cells (Fig. 6C). Thus, I supposed that GARP dependent retrograde transport is required for not only collect protein glycosylation but also lipid homeostasis.

Our results (Fig. 7 and Figs.8B and C) are consistent with previous reports showing that both tethering factors and SNAREs, especially v-SNAREs, contribute to vesicle docking and that overexpression of v-SNAREs compensates for tethering defects (VanRheenen *et al.*, 1998; Wiederkehr *et al.*, 2004; Laufman *et al.*, 2011). As discussed by Laufman et al. (Laufman *et al.*, 2011), overexpression of VAMP4 could bypass the requirement for tethering complexes (GARP in our case) because endosome-derived transport vesicles bearing highly concentrated v-SNARE proteins may directly interact with the t-SNARE complex, leading to their fusion (Laufman *et al.*, 2011). Unlike v-SNAREs, however, t-SNAREs have no such activity (Fig.7) (Laufman *et al.*, 2011). There are at least three different t-SNARE complexes in the TGN or the Golgi, STX6-STX16-Vti1, STX10-STX16-Vti1, and STX5-Ykt6-GS28. Although distinct functions for these complexes have been proposed (Mallard *et al.*, 2002; Tai *et al.*, 2004; Ganley *et al.*, 2008), there may be partial overlap such that the total amount of t-SNAREs is what allows vesicle tethering and fusion. Consistent with this speculation, the transport delay in cells with a knocked down STX6 was milder than in cells with a knocked down VAMP4 (Fig. 8E).

In previous studies, knockdown of VAMP4 or STX6 did not cause delayed

anterograde transport of $VSVG^{ts}$ (Choudhury *et al.*, 2006; Shitara *et al.*, 2013). However, I found that the anterograde transport of GPI-anchored and transmembrane reporter proteins was clearly affected by the KD of VAMP4 or STX6 (Fig. 8E). The discrepancy might be because of the different analytical methods; in the above-cited work, microscopy-based analyses were used to quantify transport efficiency whereas we used a flowcytometry-based transport assay. This allowed the simultaneous analysis of > 10,000 cells, in addition to being a more sensitive and quantitative method than microscopy. Therefore, flowcytometric analysis might be advantageous in the detection of small changes in transport efficiency, such as those seen with STX6 KD.

Mutations in the GARP complex have been described in the literature. For example, the *wobbler* mouse, used as a model for amyotrophic lateral sclerosis, has a point mutation in VPS54, leading to neurodegeneration (Schmitt-John *et al.*, 2005; Moser *et al.*, 2013). The *wobbler* mutation causes VPS54 destabilization and leads to impaired endosome-to-TGN retrograde transport (Perez-Victoria *et al.*, 2010a; Karlsson *et al.*, 2013). However, the pathogenic mechanism is yet to be elucidated. More recently, mutations in VPS53 were identified in patients with progressive cerebello-cerebral atrophy type 2 (Feinstein *et al.*, 2014). These patients display cerebellar and cerebral neuronal atrophy before the age of 1 year. The molecular mechanism leading to progressive cerebello-cerebral atrophy type 2 in patients carrying a mutation in VPS53 is also not understood. Interestingly, despite the different phenotypes of VPS53 and VPS54 mutations, motor neurons are affected in both cases (Brunet and Sacher, 2014). In human, it was reported that mutations in genes involved in anterograde transport of proteins cause motor neuronal diseases (Maruyama *et al.*, 2010; Novarino *et al.*, 2014). This study revealed the importance of the GARP complex in the post-Golgi anterograde

transport of GPI-anchored and transmembrane proteins. In addition to the retrograde transport defect itself, defective anterograde transport resulting from inefficient protein recycling from the endosome to the TGN might contribute to the pathogenic mechanism of disorders caused by VPS53 and VPS54 mutations.

I further screened genes whose overexpression restored delayed anterograde transport in V54KO cells to get specific cargo receptors for GPI-APs and identified an as yet uncharacterized gene, *TMEM87A*, encoding a member of the LU7TM family. Both TMEM87A and its close homologue TMEM87B restored delayed anterograde transport of both GPI-anchored and transmembrane proteins in V54KO cells, suggesting that they are functionally redundant and unfortunately not cargo receptors specific to GPI-APs. Microscopy analysis demonstrated the Golgi localization of TMEM87A, indicating its function at this site. This result is consistent with a previous report in which Ptm1p, the yeast homolog of TMEM87A, was identified in Tlg2p (yeast homolog of STX16)-containing compartments (Inadome *et al.*, 2005). The retrograde transport of CTxB provided proof that endosome-to-TGN transport was partially restored in V54KO+TM87A cells. Thus, restoration of the V54KO phenotype by the overexpression of TMEM87A resulted from the restoration of retrograde transport in V54KO cells and suggested the involvement of TMEM87A in endosome-to-TGN retrograde transport (Fig. 11). Retrograde transport might be a common function of LU7TM family proteins, since it also shared by GPR107, another member of this family. However, my overexpression experiments (Figs. 9A and B) evidenced two functional subfamilies, such that TMEM87A/B and GPR107/108 might be involved in different retrograde transport pathways.

Several questions regarding the precise functions of these LU7TM family

proteins and how these proteins are involved in retrograde transport remain unresolved. One possibility is that G-protein-coupled receptors (GPCRs) are needed to maintain Golgi homeostasis. In pharmacological studies, Golgi-localized Gβγ was shown to be required for post-Golgi anterograde transport (Stow *et al.*, 1991; Irannejad and Wedegaertner, 2010). However, the GPCRs associated with Golgi-localized Gβγ are not known. Tafesse et al. proposed GPR107 as one such GPCR (Tafesse *et al.*, 2014). In this study, TMEM87A/B modulated both endosome-to-TGN retrograde transport and post-Golgi anterograde transport. Thus, TMEM87A and TMEM87B are also good candidate GPCRs. Further studies are needed to elucidate the molecular function of these proteins.

In conclusion, this study showed that GARP- and VAMP4-dependent endosome-to-TGN retrograde transport is required for recycling of molecules critical for the efficient post-Golgi anterograde transport of GPI-anchored and transmembrane proteins. GPI-APs lack a cytoplasmic domain, so their efficient transport probably relies on putative transmembrane cargo receptors. Identification of cargo receptors that recognize GPI-APs would confirm this molecular mechanism.

8. Acknowledgements
We thank Dr. T. R. Brummelkamp and the Whitehead Institute for Biomedical Research for HAP1 cells; Dr. K. Horie for pCMT-SAhygpA-NP21; Drs. C. Schindler and J. S. Bonifacino for rabbit polyclonal anti-VPS52 and anti-VPS53 and expression plasmids of VPS51, VPS52, VPS53 and VPS54; Morihisa Fujita, Yoshiko Murakami, Yusuke Maeda, and Taroh Kinoshita for mentorship; Keiko Kinoshita, Yukari Onoe, and Kana Miyanagi for technical help; Kohjiro Nakamura and Yuko Kabumoto for assistance with cell sorting and Shota Nakamura, Daisuke Motooka and Kazuyoshi Gotoh for next generation sequencing. I was supported by Japan Society for the Promotion of Science (JSPS) Research Fellowship.

9. Figure legends

Figure 1. Structure and biosynthesis of GPI-APs

A. Structure of GPI-APs. Core structure of GPI is well conserved among species. GPI, composed of phosphatidylinositol, glucosamine, 3 mannoses, and 2 ethanolamine phosphates, is covalently linked to the C-terminus of proteins as a post-translational modification. GPI-APs are enriched in the lipid-rafts. B. Biosynthetic pathway of GPI. The biosynthesis of GPI is carried out in the ER through 11 stepwise reactions. After completion of assembly, GPI is covalently attached to the proteins by transamidation reaction, generating precursor of GPI-APs. C. Remodeling and transport pathway of GPI-APs. The precursor of GPI-APs generated in the ER are further remodeled in their sugar and lipid portions. In the ER, PGAP1 removes acyl chain linked to the inositol and PGAP5 removes ethanolamine phosphate attached to the 2nd mannose. These reactions are necessary for GPI-APs to bind to a p24 family complex, a cargo receptor. In the Golgi, PGAP3 removes unsaturated fatty acid from the sn2 position and PGAP2 adds saturated fatty acid at the same position.

Figure 2. Forward genetic screening of the factors required for the anterograde transport of GPI-APs. A. Enrichment of cells showing delayed VFG-GPI transport after two rounds of sorting. Transport assay of VFG-GPI in HAP1FF9 wild-type cells (left) and the cell population after sorting twice for delayed transport (right). B. Bubble plot of enriched gene-trap insertion numbers after two rounds of sorting. The significance of enrichment was calculated by comparing the numbers of insertions in each gene before and after two rounds of sorting and plotted. The horizontal line shows the chromosomal position of the genes, and the vertical line the significance of enrichment of each gene

(*P* value). The size of the bubble shows the number of inactivating insertion sites (IAIS). Genes significantly enriched in Sort 2 ($P<0.01$) are colored. Red bubbles indicated genes encoding the GARP complex subunits and green bubbles the genes involved in the remodeling of GPI-APs. The bubble of VPS53 indicated by arrow was close to the significance limit.

Figure 3. Knockout (KO) of GARP complex subunits severely impairs the anterograde transport of proteins. A. Western blotting of VPS52 and VPS53 in HEK293FF6 wild-type (WT), VPS52-KO (V52KO) and VPS53-KO (V53KO) cells, showing nearly complete reduction by specific KO. GAPDH was used as a loading control. B. Transport assay of VFG-GPI in WT and GARP-KO cells. Surface expression of VFG-GPI at the indicated time in WT and VPS54-KO (V54KO) cells was shown as an example. C. Relative transport of VFG-GPI in GARP-KO cells. The geometric mean fluorescence of surface VFG-GPI at each time point, determined from the histograms shown in (B), was plotted as a function of time, using the geometric mean of WT cells at 90 min as 100% relative transport. Data are the means of three independent experiments. Error bars represent the SDs (n=3). D. Transport assay of FVG-TM in WT and GARP-KO cells. WT and GARP-KO cells were transiently transfected with FVG-TM. Surface expression of FVG-TM at the indicated time in WT and V54KO cells was shown as an example. E. Relative transport of FVG-TM. The geometric mean fluorescence of surface FVG-TM, determined from the histograms shown in (D), was plotted similarly to (C). Data are the means of three independent experiments. Error bars represent the SDs (n=3). F. Rescue of transport delay in GARP-KO cells by the expression of the responsible genes. GARP-KO cells were transiently transfected with

VPS51, VPS52, VPS53, or VPS54 expression plasmid, after which the transport of VFG-GPI (left) was analyzed. For FVG-TM transport (right), cells were cotransfected with FVG-TM and indicated genes for rescue.

Figure 4. Post-Golgi anterograde transport is defective in V54KO cells. A. VFG-GPI transport from the ER in V54KO or restored cells. Cells were cultured in medium containing 1 μg/ml Dox at 40°C for 24 h. VFG-GPI transport was chased at 32°C for the indicated time in medium containing 100 μg/ml CHX. Images at 0, 30, and 90 min are shown. Green, VFG-GPI; red, RFP-GPP34 as a TGN marker. Scale bars, 10 μm. B. The TGN localization of VFG-GPI was quantified based on (A). The ratio of the VFG-GPI intensity in the TGN to the total fluorescence intensity was determined. Data are the means of 10 independent images. Error bars represent the SEM (n=10). Similar results were obtained from two independent experiments. C. Post-Golgi transport of VFG-GPI in V54KO or restored cells. Cells cultured in medium containing 1 μg/ml Dox for 24 h at 40°C were pre-cultured in medium containing 100 μg/ml CHX for 3 h at 19°C; after which VFG-GPI transport was chased at 32°C for 0 or 45 min. To detect surface VFG-GPI, cells were stained with anti-FLAG M2 antibody under non-permeabilized conditions. Green, total expression of VFG-GPI; red, RFP-GPP34; cyan, surface expression of VFG-GPI. Scale bars, 10 μm. Similar results were obtained from two independent experiments. D. The ratio of surface arrived VFG-GPI was quantified based on (C). Data are the means of 10 independent images. Error bars represent the SEM (n=5). Similar results were obtained from two independent experiments.

Figure 5. Missorting of CD59 to lysosomes in V54KO cells. A. Intracellular localization of endogenous GPI-AP, CD59. Cells were treated with PI-PLC at 37°C for 1.5 h after which fixed and double stained with anti-CD59 and anti-LAMP1 or anti-EEA1. Green, CD59; red, LAMP1 (upper panels) and EEA1 (lower panels) as lysosome and early-endosome markers, respectively. Scale bars, 10 μm. B. CD59 localized in lysosomes was quantified from the images of (A). Data are the means of 10 independent images. Error bars represent the SEM (n=10). Similar results were obtained in two independent experiments. C. Relative surface expression of CD59 in V54KO cells and restored cells. Surface expression of CD59 was analyzed by flowcytometry. The geometric mean fluorescence of surface CD59 in cells was quantified and relative expression was calculated. Error bars represent the SDs (n=2).

Figure 6. Depletion of GARP complex impaired O-glycosylation but not N-glycosylation. A. Surface glycosylation profiles of V54KO cells. Cells were stained using FITC-conjugated lectins or Alexa Flour 488-conjugated CTxB and analyzed by flowcytometry. The geometric mean fluorescence was quantified for each probe and relative expression was calculated. Error bars represent the SDs (n=2 for Con A, n=3 for WGA, LCA, and MAM, and n=4 for SBA, PNA, UEA-I and CTxB). B. Western blotting of several glycoproteins in GARP-KO cells. TfR, DAF, and LAMP1 were detected. GAPDH was used as a loading control. Arrows represented abnormal glycosylation form of proteins. C. Confocal images with CTxB. Cells were fixed and double stained with CTxB and anti-GPP130 antibody under pearmeabilized conditions. Green, CTxB; red, GPP130 as a Golgi marker. Scale bars, 10 μm.

Figure 7. Overexpression of VAMP4 partially restored the anterograde defect in V54KO cells. Transport assay of VFG-GPI (left) and FVG-TM (right) in V54KO cells transiently transfected with the indicated genes. Surface expression levels of VFG-GPI and FVG-GPI at the indicated time were shown.

Figure 8. VAMP4-dependent retrograde transport is required for recycling of proteins critical for the post-Golgi anterograde transport. A. Transport assay in V54KO cells stably expressing VAMP4 (V54KO+VAMP4). V54KO+VAMP4 cells in which the anterograde transport of VFG-GPI was efficiently restored were collected twice by cell sorting. After cell sorting, transport assay was conducted. B. Retrograde transport assay using CTxB. Cells incubated with Alexa Fluor 488-conjugated CTxB for 30 min on ice followed by a chase at 37°C for 0 or 60 min were analyzed by confocal microscopy after staining with anti-Golgin97 antibody. Green, CTxB; red, Golgin97 as a TGN marker. Scale bars, 10 μm. Similar results were obtained in two independent experiments. C. CTxB in the TGN was quantified. Data are the means of 10 independent images. Error bars represent the SEM (n=10). Similar results were obtained in two independent experiments. D. Estimation of knockdown efficiency. HEK293FF6 was transfected with indicated siRNAs and the expression of STX6 or VAMP4 were analyzed by Western blotting or qRT-PCR, respectively. For Western blotting, α-tubulin was used as a loading control. For qRT-PCR, HPRT1 was used as a control. #1 and #2 represent siRNAs targeting different sites. E. Effect of STX6 or VAMP4 knockdown on anterograde transport. Transport assay of VFG-GPI (left) or FVG-TM (right) in HEK293FF6 or HEK293TM10 cells, respectively, transfected with indicated siRNAs.

Figure 9. Potential role for TMEM87A and TMEM87B in endosome-to-TGN retrograde transport. A. Overexpression of TMEM87A (TM87A) and TMEM87B (TM87B) partially rescued the delayed transport of proteins in V54KO cells. Transport assay of VFG-GPI (left) or FVG-TM (right) in V54KO cells transiently transfected with the indicated genes. B. Overexpression of GPR107 and GPR108 did not rescue delayed transport in V54KO cells. Transport assay of VFG-GPI (left) or FVG-TM (right) in V54KO cells transfected with the indicated genes. C. Subcellular localization of TM87A. Wild-type cells were transfected with non-tagged or HA-tagged TM87A and double-stained with anti-TMEM87A (non-tagged version) or anti-HA7 and anti-GPP130. Green, TMEM87A; red, GPP130 as a Golgi marker. Scale bars, 10 μm. D. Transport assay in V54KO cells stably expressing HA-TM87A (V54KO+TM87A). V54KO+TM87A in which the anterograde transport of VFG-GPI was efficiently restored were collected twice by cell sorting. After cell sorting, transport assay was conducted. E. CTxB retrograde transport at 0 min and 60 min. Green, CTxB; red, Golgin97. Scale bars, 10 μm. Similar results were obtained in two independent experiments. F. Quantitative data were obtained as described in Fig. 8C legend. Data are the means of 10 independent images. Error bars represent SEM (n=10). Similar results were obtained in two independent experiments.

Figure 10. Double KO of TMEM87A and TMEM87B did not impair endosome-to-TGN retrograde tranposrt of CTxB. A. Relative expression of TMEM87A and B in wild-type HEK293 cells. The expression of TMEM87A and B relative to HPRT1 expression was analyzed by qRT-PCR. Both TMEM87A and B were express at

levels comparable to VPS51 and VPS54 in HEK293 cells. B. Retrograde transport assay in TMEM87A- and TMEM87B-double KO HEK293 cells using CTxB. CTxB retrograde transport at 0, 15, and 30 min in wild-type HEK293 cells and TMEM87A/B-double KO HEK293 cells were similar.

Figure 11. Proposed model of the post-Golgi anterograde transport of proteins. 1. Cell surface integral membrane proteins are sorted and packaged in transport vesicles in a process mediated by putative cargo receptors. 2. The proteins are then transported to the plasma membrane together with the cargo receptors. 3. After dissociation of the proteins from the cargo receptors at the cell surface, the cargo receptors are endocytosed and delivered to early endosome (EE) or the recycling endosome (RE). 4. The cargo receptors are recycled back to the Golgi for further round of anterograde transport via endosome-to-TGN retrograde transport mediated by VAMP4, GARP complex and STX6. TMEM87A might be involved in this recycling step.

10. References

Belden, W.J., and Barlowe, C. (1996). Erv25p, a component of COPII-coated vesicles, forms a complex with Emp24p that is required for efficient endoplasmic reticulum to Golgi transport. J Biol Chem *271*, 26939-26946.

Belenkaya, T.Y., Wu, Y., Tang, X., Zhou, B., Cheng, L., Sharma, Y.V., Yan, D., Selva, E.M., and Lin, X. (2008). The retromer complex influences Wnt secretion by recycling wntless from endosomes to the trans-Golgi network. Dev Cell *14*, 120-131.

Bonifacino, J.S., and Glick, B.S. (2004). The mechanisms of vesicle budding and fusion. Cell *116*, 153-166.

Bonifacino, J.S., and Hierro, A. (2011). Transport according to GARP: receiving retrograde cargo at the trans-Golgi network. Trends Cell Biol *21*, 159-167.

Bonnon, C., Wendeler, M.W., Paccaud, J.P., and Hauri, H.P. (2010). Selective export of human GPI-anchored proteins from the endoplasmic reticulum. J Cell Sci *123*, 1705-1715.

Brandizzi, F., and Barlowe, C. (2013). Organization of the ER-Golgi interface for membrane traffic control. Nat Rev Mol Cell Biol *14*, 382-392.

Brunet, S., and Sacher, M. (2014). In sickness and in health: the role of TRAPP and associated proteins in disease. Traffic *15*, 803-818.

Calakos, N., Bennett, M.K., Peterson, K.E., and Scheller, R.H. (1994). Protein-protein interactions contributing to the specificity of intracellular vesicular trafficking. Science *263*, 1146-1149.

Carette, J.E., Guimaraes, C.P., Wuethrich, I., Blomen, V.A., Varadarajan, M., Sun, C., Bell, G., Yuan, B., Muellner, M.K., Nijman, S.M., Ploegh, H.L., and Brummelkamp, T.R. (2011a). Global gene disruption in human cells to assign genes to phenotypes by deep sequencing. Nat Biotechnol *29*, 542-546.

Carette, J.E., Raaben, M., Wong, A.C., Herbert, A.S., Obernosterer, G., Mulherkar, N., Kuehne, A.I., Kranzusch, P.J., Griffin, A.M., Ruthel, G., Dal Cin, P., Dye, J.M., Whelan, S.P., Chandran, K., and Brummelkamp, T.R. (2011b). Ebola virus entry requires the cholesterol transporter Niemann-Pick C1. Nature *477*, 340-343.

Carney, G.E., and Bowen, N.J. (2004). p24 proteins, intracellular trafficking, and behavior: Drosophila melanogaster provides insights and opportunities. Biol Cell *96*, 271-278.

Chen, Y.A., and Scheller, R.H. (2001). SNARE-mediated membrane fusion. Nat Rev

Mol Cell Biol *2*, 98-106.
Chia, P.Z., Gunn, P., and Gleeson, P.A. (2013). Cargo trafficking between endosomes and the trans-Golgi network. Histochem Cell Biol *140*, 307-315.
Choudhury, A., Marks, D.L., Proctor, K.M., Gould, G.W., and Pagano, R.E. (2006). Regulation of caveolar endocytosis by syntaxin 6-dependent delivery of membrane components to the cell surface. Nat Cell Biol *8*, 317-328.
Climer, L.K., Dobretsov, M., and Lupashin, V. (2015). Defects in the COG complex and COG-related trafficking regulators affect neuronal Golgi function. Front Neurosci *9*, 405.
Cong, L., Ran, F.A., Cox, D., Lin, S., Barretto, R., Habib, N., Hsu, P.D., Wu, X., Jiang, W., Marraffini, L.A., and Zhang, F. (2013). Multiplex genome engineering using CRISPR/Cas systems. Science *339*, 819-823.
Conibear, E., and Stevens, T.H. (2000). Vps52p, Vps53p, and Vps54p form a novel multisubunit complex required for protein sorting at the yeast late Golgi. Mol Biol Cell *11*, 305-323.
Dominguez, M., Dejgaard, K., Fullekrug, J., Dahan, S., Fazel, A., Paccaud, J.P., Thomas, D.Y., Bergeron, J.J., and Nilsson, T. (1998). gp25L/emp24/p24 protein family members of the cis-Golgi network bind both COP I and II coatomer. J Cell Biol *140*, 751-765.
Elling, U., Taubenschmid, J., Wirnsberger, G., O'Malley, R., Demers, S.P., Vanhaelen, Q., Shukalyuk, A.I., Schmauss, G., Schramek, D., Schnuetgen, F., von Melchner, H., Ecker, J.R., Stanford, W.L., Zuber, J., Stark, A., and Penninger, J.M. (2011). Forward and reverse genetics through derivation of haploid mouse embryonic stem cells. Cell Stem Cell *9*, 563-574.
Feinstein, M., Flusser, H., Lerman-Sagie, T., Ben-Zeev, B., Lev, D., Agamy, O., Cohen, I., Kadir, R., Sivan, S., Leshinsky-Silver, E., Markus, B., and Birk, O.S. (2014). VPS53 mutations cause progressive cerebello-cerebral atrophy type 2 (PCCA2). J Med Genet *51*, 303-308.
Franch-Marro, X., Wendler, F., Guidato, S., Griffith, J., Baena-Lopez, A., Itasaki, N., Maurice, M.M., and Vincent, J.P. (2008). Wingless secretion requires endosome-to-Golgi retrieval of Wntless/Evi/Sprinter by the retromer complex. Nat Cell Biol *10*, 170-177.
Frohlich, F., Petit, C., Kory, N., Christiano, R., Hannibal-Bach, H.K., Graham, M., Liu,

X., Ejsing, C.S., Farese, R.V., and Walther, T.C. (2015). The GARP complex is required for cellular sphingolipid homeostasis. Elife *4*.
Fujita, M., Maeda, Y., Ra, M., Yamaguchi, Y., Taguchi, R., and Kinoshita, T. (2009). GPI glycan remodeling by PGAP5 regulates transport of GPI-anchored proteins from the ER to the Golgi. Cell *139*, 352-365.
Fujita, M., Watanabe, R., Jaensch, N., Romanova-Michaelides, M., Satoh, T., Kato, M., Riezman, H., Yamaguchi, Y., Maeda, Y., and Kinoshita, T. (2011). Sorting of GPI-anchored proteins into ER exit sites by p24 proteins is dependent on remodeled GPI. J Cell Biol *194*, 61-75.
Ganley, I.G., Espinosa, E., and Pfeffer, S.R. (2008). A syntaxin 10-SNARE complex distinguishes two distinct transport routes from endosomes to the trans-Golgi in human cells. J Cell Biol *180*, 159-172.
Harterink, M., Port, F., Lorenowicz, M.J., McGough, I.J., Silhankova, M., Betist, M.C., van Weering, J.R., van Heesbeen, R.G., Middelkoop, T.C., Basler, K., Cullen, P.J., and Korswagen, H.C. (2011). A SNX3-dependent retromer pathway mediates retrograde transport of the Wnt sorting receptor Wntless and is required for Wnt secretion. Nat Cell Biol *13*, 914-923.
Hong, W., and Lev, S. (2013). Tethering the assembly of SNARE complexes. Trends Cell Biol *24*, 35-43.
Horie, K., Kokubu, C., Yoshida, J., Akagi, K., Isotani, A., Oshitani, A., Yusa, K., Ikeda, R., Huang, Y., Bradley, A., and Takeda, J. (2011). A homozygous mutant embryonic stem cell bank applicable for phenotype-driven genetic screening. Nat Methods *8*, 1071-1077.
Inadome, H., Noda, Y., Adachi, H., and Yoda, K. (2005). Immunoisolaton of the yeast Golgi subcompartments and characterization of a novel membrane protein, Svp26, discovered in the Sed5-containing compartments. Mol Cell Biol *25*, 7696-7710.
Irannejad, R., and Wedegaertner, P.B. (2010). Regulation of constitutive cargo transport from the trans-Golgi network to plasma membrane by Golgi-localized G protein betagamma subunits. J Biol Chem *285*, 32393-32404.
Jaensch, N., Correa, I.R., Jr., and Watanabe, R. (2014). Stable cell surface expression of GPI-anchored proteins, but not intracellular transport, depends on their fatty acid structure. Traffic *15*, 1305-1329.
Kal, A.J., van Zonneveld, A.J., Benes, V., van den Berg, M., Koerkamp, M.G.,

Albermann, K., Strack, N., Ruijter, J.M., Richter, A., Dujon, B., Ansorge, W., and Tabak, H.F. (1999). Dynamics of gene expression revealed by comparison of serial analysis of gene expression transcript profiles from yeast grown on two different carbon sources. Mol Biol Cell *10*, 1859-1872.

Karlsson, P., Droce, A., Moser, J.M., Cuhlmann, S., Padilla, C.O., Heimann, P., Bartsch, J.W., Fuchtbauer, A., Fuchtbauer, E.M., and Schmitt-John, T. (2013). Loss of vps54 function leads to vesicle traffic impairment, protein mis-sorting and embryonic lethality. Int J Mol Sci *14*, 10908-10925.

Kinoshita, T., Fujita, M., and Maeda, Y. (2008). Biosynthesis, remodelling and functions of mammalian GPI-anchored proteins: recent progress. J Biochem *144*, 287-294.

Laufman, O., Hong, W., and Lev, S. (2011). The COG complex interacts directly with Syntaxin 6 and positively regulates endosome-to-TGN retrograde transport. J Cell Biol *194*, 459-472.

Maeda, Y., Ide, T., Koike, M., Uchiyama, Y., and Kinoshita, T. (2008). GPHR is a novel anion channel critical for acidification and functions of the Golgi apparatus. Nat Cell Biol *10*, 1135-1145.

Maeda, Y., Tashima, Y., Houjou, T., Fujita, M., Yoko-o, T., Jigami, Y., Taguchi, R., and Kinoshita, T. (2007). Fatty acid remodeling of GPI-anchored proteins is required for their raft association. Mol Biol Cell *18*, 1497-1506.

Mali, P., Yang, L., Esvelt, K.M., Aach, J., Guell, M., DiCarlo, J.E., Norville, J.E., and Church, G.M. (2013). RNA-guided human genome engineering via Cas9. Science *339*, 823-826.

Mallard, F., Antony, C., Tenza, D., Salamero, J., Goud, B., and Johannes, L. (1998). Direct pathway from early/recycling endosomes to the Golgi apparatus revealed through the study of shiga toxin B-fragment transport. J Cell Biol *143*, 973-990.

Mallard, F., Tang, B.L., Galli, T., Tenza, D., Saint-Pol, A., Yue, X., Antony, C., Hong, W., Goud, B., and Johannes, L. (2002). Early/recycling endosomes-to-TGN transport involves two SNARE complexes and a Rab6 isoform. J Cell Biol *156*, 653-664.

Maruyama, H., Morino, H., Ito, H., Izumi, Y., Kato, H., Watanabe, Y., Kinoshita, Y., Kamada, M., Nodera, H., Suzuki, H., Komure, O., Matsuura, S., Kobatake, K., Morimoto, N., Abe, K., Suzuki, N., Aoki, M., Kawata, A., Hirai, T., Kato, T., Ogasawara, K., Hirano, A., Takumi, T., Kusaka, H., Hagiwara, K., Kaji, R., and

Kawakami, H. (2010). Mutations of optineurin in amyotrophic lateral sclerosis. Nature *465*, 223-226.
Matlin, K.S., and Simons, K. (1983). Reduced temperature prevents transfer of a membrane glycoprotein to the cell surface but does not prevent terminal glycosylation. Cell *34*, 233-243.
Moser, J.M., Bigini, P., and Schmitt-John, T. (2013). The wobbler mouse, an ALS animal model. Mol Genet Genomics *288*, 207-229.
Nishimoto-Morita, K., Shin, H.W., Mitsuhashi, H., Kitamura, M., Zhang, Q., Johannes, L., and Nakayama, K. (2009). Differential effects of depletion of ARL1 and ARFRP1 on membrane trafficking between the trans-Golgi network and endosomes. J Biol Chem *284*, 10583-10592.
Novarino, G., Fenstermaker, A.G., Zaki, M.S., Hofree, M., Silhavy, J.L., Heiberg, A.D., Abdellateef, M., Rosti, B., Scott, E., Mansour, L., Masri, A., Kayserili, H., Al-Aama, J.Y., Abdel-Salam, G.M., Karminejad, A., Kara, M., Kara, B., Bozorgmehri, B., Ben-Omran, T., Mojahedi, F., Mahmoud, I.G., Bouslam, N., Bouhouche, A., Benomar, A., Hanein, S., Raymond, L., Forlani, S., Mascaro, M., Selim, L., Shehata, N., Al-Allawi, N., Bindu, P.S., Azam, M., Gunel, M., Caglayan, A., Bilguvar, K., Tolun, A., Issa, M.Y., Schroth, J., Spencer, E.G., Rosti, R.O., Akizu, N., Vaux, K.K., Johansen, A., Koh, A.A., Megahed, H., Durr, A., Brice, A., Stevanin, G., Gabriel, S.B., Ideker, T., and Gleeson, J.G. (2014). Exome sequencing links corticospinal motor neuron disease to common neurodegenerative disorders. Science *343*, 506-511.
Oka, T., Ungar, D., Hughson, F.M., and Krieger, M. (2004). The COG and COPI complexes interact to control the abundance of GEARs, a subset of Golgi integral membrane proteins. Mol Biol Cell *15*, 2423-2435.
Olson, A.L., Knight, J.B., and Pessin, J.E. (1997). Syntaxin 4, VAMP2, and/or VAMP3/cellubrevin are functional target membrane and vesicle SNAP receptors for insulin-stimulated GLUT4 translocation in adipocytes. Mol Cell Biol *17*, 2425-2435.
Ong, Y.S., Tran, T.H., Gounko, N.V., and Hong, W. (2014). TMEM115 is an integral membrane protein of the Golgi complex involved in retrograde transport. J Cell Sci *127*, 2825-2839.
Paladino, S., Sarnataro, D., Pillich, R., Tivodar, S., Nitsch, L., and Zurzolo, C. (2004). Protein oligomerization modulates raft partitioning and apical sorting of GPI-anchored proteins. J Cell Biol *167*, 699-709.

Paladino, S., Sarnataro, D., Tivodar, S., and Zurzolo, C. (2007). Oligomerization is a specific requirement for apical sorting of glycosyl-phosphatidylinositol-anchored proteins but not for non-raft-associated apical proteins. Traffic *8*, 251-258.
Pastor-Cantizano, N., Montesinos, J.C., Bernat-Silvestre, C., Marcote, M.J., and Aniento, F. (2015). p24 family proteins: key players in the regulation of trafficking along the secretory pathway. Protoplasma.
Pepperkok, R., Scheel, J., Horstmann, H., Hauri, H.P., Griffiths, G., and Kreis, T.E. (1993). Beta-COP is essential for biosynthetic membrane transport from the endoplasmic reticulum to the Golgi complex in vivo. Cell *74*, 71-82.
Perez-Victoria, F.J., Abascal-Palacios, G., Tascon, I., Kajava, A., Magadan, J.G., Pioro, E.P., Bonifacino, J.S., and Hierro, A. (2010a). Structural basis for the wobbler mouse neurodegenerative disorder caused by mutation in the Vps54 subunit of the GARP complex. Proc Natl Acad Sci U S A *107*, 12860-12865.
Perez-Victoria, F.J., Mardones, G.A., and Bonifacino, J.S. (2008). Requirement of the human GARP complex for mannose 6-phosphate-receptor-dependent sorting of cathepsin D to lysosomes. Mol Biol Cell *19*, 2350-2362.
Perez-Victoria, F.J., Schindler, C., Magadan, J.G., Mardones, G.A., Delevoye, C., Romao, M., Raposo, G., and Bonifacino, J.S. (2010b). Ang2/fat-free is a conserved subunit of the Golgi-associated retrograde protein complex. Mol Biol Cell *21*, 3386-3395.
Peter, F., Plutner, H., Zhu, H., Kreis, T.E., and Balch, W.E. (1993). Beta-COP is essential for transport of protein from the endoplasmic reticulum to the Golgi in vitro. J Cell Biol *122*, 1155-1167.
Schimmoller, F., Singer-Kruger, B., Schroder, S., Kruger, U., Barlowe, C., and Riezman, H. (1995). The absence of Emp24p, a component of ER-derived COPII-coated vesicles, causes a defect in transport of selected proteins to the Golgi. EMBO J *14*, 1329-1339.
Schindler, C., Chen, Y., Pu, J., Guo, X., and Bonifacino, J.S. (2015). EARP is a multisubunit tethering complex involved in endocytic recycling. Nat Cell Biol *17*, 639-650.
Schmitt-John, T., Drepper, C., Mussmann, A., Hahn, P., Kuhlmann, M., Thiel, C., Hafner, M., Lengeling, A., Heimann, P., Jones, J.M., Meisler, M.H., and Jockusch, H. (2005). Mutation of Vps54 causes motor neuron disease and defective spermiogenesis

in the wobbler mouse. Nat Genet *37*, 1213-1215.
Seong, J., Wang, Y., Kinoshita, T., and Maeda, Y. (2013). Implications of lipid moiety in oligomerization and immunoreactivities of GPI-anchored proteins. J Lipid Res *54*, 1077-1091.
Shaner, N.C., Lin, M.Z., McKeown, M.R., Steinbach, P.A., Hazelwood, K.L., Davidson, M.W., and Tsien, R.Y. (2008). Improving the photostability of bright monomeric orange and red fluorescent proteins. Nat Methods *5*, 545-551.
Shitara, A., Shibui, T., Okayama, M., Arakawa, T., Mizoguchi, I., Sakakura, Y., and Takuma, T. (2013). VAMP4 is required to maintain the ribbon structure of the Golgi apparatus. Mol Cell Biochem *380*, 11-21.
Simons, K., and van Meer, G. (1988). Lipid sorting in epithelial cells. Biochemistry *27*, 6197-6202.
Siniossoglou, S., and Pelham, H.R. (2002). Vps51p links the VFT complex to the SNARE Tlg1p. J Biol Chem *277*, 48318-48324.
Spaapen, L.J., Bakker, J.A., van der Meer, S.B., Sijstermans, H.J., Steet, R.A., Wevers, R.A., and Jaeken, J. (2005). Clinical and biochemical presentation of siblings with COG-7 deficiency, a lethal multiple O- and N-glycosylation disorder. J Inherit Metab Dis *28*, 707-714.
Stow, J.L., de Almeida, J.B., Narula, N., Holtzman, E.J., Ercolani, L., and Ausiello, D.A. (1991). A heterotrimeric G protein, G alpha i-3, on Golgi membranes regulates the secretion of a heparan sulfate proteoglycan in LLC-PK1 epithelial cells. J Cell Biol *114*, 1113-1124.
Strating, J.R., and Martens, G.J. (2009). The p24 family and selective transport processes at the ER-Golgi interface. Biol Cell *101*, 495-509.
Tafesse, F.G., Guimaraes, C.P., Maruyama, T., Carette, J.E., Lory, S., Brummelkamp, T.R., and Ploegh, H.L. (2014). GPR107, a G-protein-coupled receptor essential for intoxication by Pseudomonas aeruginosa exotoxin A, localizes to the Golgi and is cleaved by furin. J Biol Chem *289*, 24005-24018.
Tai, G., Lu, L., Wang, T.L., Tang, B.L., Goud, B., Johannes, L., and Hong, W. (2004). Participation of the syntaxin 5/Ykt6/GS28/GS15 SNARE complex in transport from the early/recycling endosome to the trans-Golgi network. Mol Biol Cell *15*, 4011-4022.
Takida, S., Maeda, Y., and Kinoshita, T. (2008). Mammalian GPI-anchored proteins require p24 proteins for their efficient transport from the ER to the plasma membrane.

Biochem J *409*, 555-562.
Tanaka, S., Maeda, Y., Tashima, Y., and Kinoshita, T. (2004). Inositol deacylation of glycosylphosphatidylinositol-anchored proteins is mediated by mammalian PGAP1 and yeast Bst1p. J Biol Chem *279*, 14256-14263.
Tashima, Y., Taguchi, R., Murata, C., Ashida, H., Kinoshita, T., and Maeda, Y. (2006). PGAP2 is essential for correct processing and stable expression of GPI-anchored proteins. Mol Biol Cell *17*, 1410-1420.
Theiler, R., Fujita, M., Nagae, M., Yamaguchi, Y., Maeda, Y., and Kinoshita, T. (2014). The alpha-helical region in p24gamma2 subunit of p24 protein cargo receptor is pivotal for the recognition and transport of glycosylphosphatidylinositol-anchored proteins. J Biol Chem *289*, 16835-16843.
Ungar, D., Oka, T., Krieger, M., and Hughson, F.M. (2006). Retrograde transport on the COG railway. Trends Cell Biol *16*, 113-120.
van Meer, G., Stelzer, E.H., Wijnaendts-van-Resandt, R.W., and Simons, K. (1987). Sorting of sphingolipids in epithelial (Madin-Darby canine kidney) cells. J Cell Biol *105*, 1623-1635.
VanRheenen, S.M., Cao, X., Lupashin, V.V., Barlowe, C., and Waters, M.G. (1998). Sec35p, a novel peripheral membrane protein, is required for ER to Golgi vesicle docking. J Cell Biol *141*, 1107-1119.
Wiederkehr, A., De Craene, J.O., Ferro-Novick, S., and Novick, P. (2004). Functional specialization within a vesicle tethering complex: bypass of a subset of exocyst deletion mutants by Sec1p or Sec4p. J Cell Biol *167*, 875-887.
Wu, X., Steet, R.A., Bohorov, O., Bakker, J., Newell, J., Krieger, M., Spaapen, L., Kornfeld, S., and Freeze, H.H. (2004). Mutation of the COG complex subunit gene COG7 causes a lethal congenital disorder. Nat Med *10*, 518-523.
Zhou, G.L., Na, S.Y., Niedra, R., and Seed, B. (2014). Deficits in receptor-mediated endocytosis and recycling in cells from mice with Gpr107 locus disruption. J Cell Sci *127*, 3916-3927.

Table: List of KO cells

gene	cell	DNA sequence	amino acid sequence
VPS51	wild-type	GGCCCGAGGGGGAGGCTCCGGAGCGTCGGCGGAAGGCGCACGGGATG	MAAAAAAGPSPGSGPGDSPEGPEGEAPERRRKAHGM
	V51 KO	GGCCCGAGGGGGAGGCTCCGGAGCGTGCGGCGGAAGGCGCACGGGATG	MAAAAAAGPSPGSGPGDSPEGPEGEAPERAAEGARDAEALLRPLGRGGGGTPRGARPPGPD*
		GGCCCGAGGGGGAGGCTCCGGAG--------GAAGGCGCACGGGATG	MAAAAAAGPSPGSGPGDSPEGPEGEAPEEGARDAEALLRPLGRGGGGTPRGARPPGPD*
VPS52	wild-type	GCGGCTGCGGCCCGGGAACTGGTGTTGCGGGCTGGGACCTCAGA	MAAAATMAAAARELVLRAGTS
	V52 KO	GCGGCTGCGGCCCGGGAACTGGGTGGTATTGGCGGCAA… GCGTTAGATGAGGTATCCTTGCGGGCTGGGACCTCAGA	MAAAATMAAAARELGGIGGNQQQIRDANLLCCGGLQRGEQGVR*
		GCGGCTGCGGCCCGGGAACTGGTGTATTGACGTCAATGGGTGGGGGTCGT TGGGC…	MAAAATMAAAARELVY*
VPS53	wild-type	AGCCGTGCTGCAGCTCACGCCCGAGGTGCAGCTGGCCATCGAGCAG	MMEEEELEFVEELEAVLQLTPEVQLAIEQ
	V53 KO	AGCCGTGCTGCAGCTCACGCCCGAGGTG-AGCTGGCCATCGAGCAG	MMEEEELEFVEELEAVLQLTPEVSWPSSRCFQARTL*
		AGCCGTGCTGCAGCTCACGCCCGAGGTGCGTGATGCTCGT… GGGTGATGGTTCAGCTGGCCATCGAGCAG	MMEEEELEFVEELEAVLQLTPEVRDARQGGGTRQD…PVTIVLSPTR*
		AGCCGTGCTGCAGCTCACGCCCGAGGTGCTTTTGCTGGC… CCAGCAGGCCAGCTGGCCATCGAGCAG	MMEEEELEFVEELEAVLQLTPEVLLLAFCSHVRAYFP*
VPS54	wild-type	ATGGCTTCAAGCCACAGTTCTTCACCAGTGCCTCAAGGAAGCAGCA… ATTCGACCTGTGCCATCACTGCCAGATGTGTGTCCCAAGGAACCCACAG	MASSHSSSPVPQGSSSDVFFKIEVDPSKHIRPVPSLPDVCPKEPT
	V54 KO	ATGGCTTCAAGCCACAGCTGCCAGATGTGTGTCCCAAGGAACCCACAG	MASSHSCQMCVPRNPQVIHIVYMLPHL*
		ATGGCTTCAAGCCACAGCAGCAGATTCGCCTGGATGACCAGAAAGAGCGA GGAAACCACTGCCAGATGTGTGTCCCAAGGAACCCACAG	MASSHSSRFAWMTRKSEETTARCVSQGTHR*
TMEM87A	wild-type	GCTAAGGAGAATGGAACAAACCTTACCTTTATTGGAGACAAAACC	MAAAAWLQVL…AKENGTNLTFIGDKTAMHEPL
	TM87A, B-DKO #1	GCTAAGGAGAATGGAACAAACCTTACCTT-ATTGGAGACAAAACC	MAAAAWLQVL…AKENGTNLTLETKPQCMNHCKLGKMHHTFLLYILAFHPQRNHQKKIH*
	TM87A, B-DKO #2	GCTAAGGAGAATGGAACAAACCTTACCTT-ATTGGAGACAAAACC	MAAAAWLQVL…AKENGTNLTLETKPQCMNHCKLGKMHHTFLLYILAFHPQRNHQKKIH*
TMEM87B	wild-type	GGCTCCTGCCACGCCGCCGCCGCTGCTTTCCCGCCCGGGCCCCGCTGC TGCGCGTCGCCCTC	MVAACRSV…LCWTPAAVRAVPELGLWL
	TM87A, B-DKO #1	GGCTCCTGCCACGCCGCCGCCGCTGCTTTCCCGGTGCTCCAGGTAATTA AACATTAATACCCCACCAACCAACGCCCGGGCCCCGCTGCTGCGCGTCGC CCTC	MVAACRS…PRRRRCFPGAPGN*
		GGCTCCTGCCACGCCGCCGCCGCTGCTTTCCCCGCCCGGGCCCCGCTGC TGCGCGTCGCCCTC	MVAACRS…PRRRRCFPRPGPAAARRPLPPVLDPGGCARGP*
		GGCTCCTGCCACGCCGCCGCCGCTGCTTTCCC---------- -GCGCGTCGCCCTC	MVAACRS…PRRRRCFPARRPLPPVLDPGGCARGP*
	wild-type	CTGTGCTGGACCCCGGCGGCTGTGCGCGCGGTCCCTGAGCTCGGGCTC	MVAACRSV…LCWTPAAVRAVPELGLWL
	TM87A, B-DKO #2	CTGTGCTGGACCCCGGCGGCTGTGCCGCGCGGTCCCTGAGCTCGGGCTC	MVAACRSV…LCWTPAAVPRGP*
		CTGTGCTGGACCCCGGCGGCTGTGCACGCGCGGTCCCTGAGCTCGGGCTC	MVAACRSV…LCWTPAAVHARSLSSGSG*

* : stop

12. Figures

Fig. 1

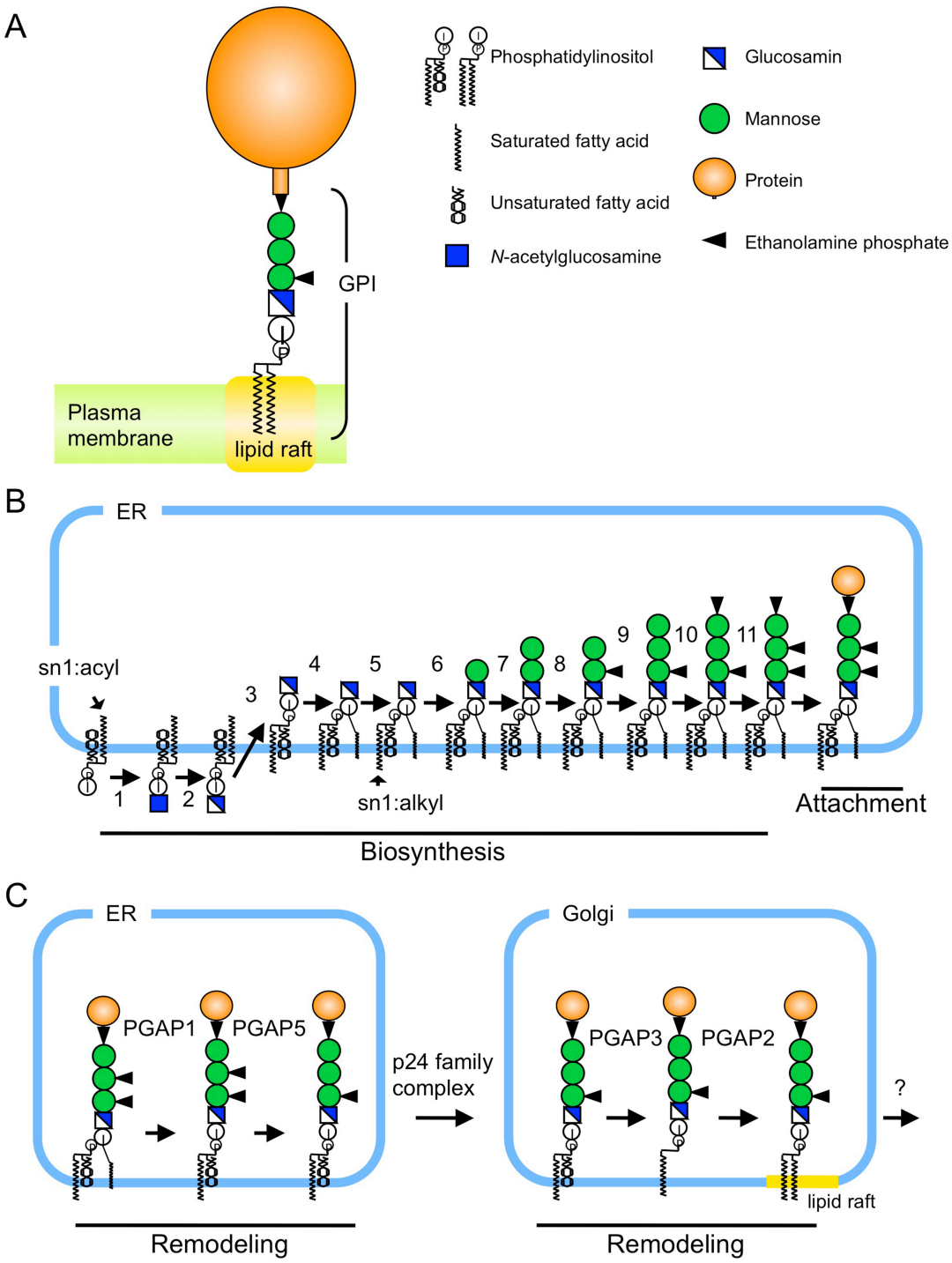

Fig. 2

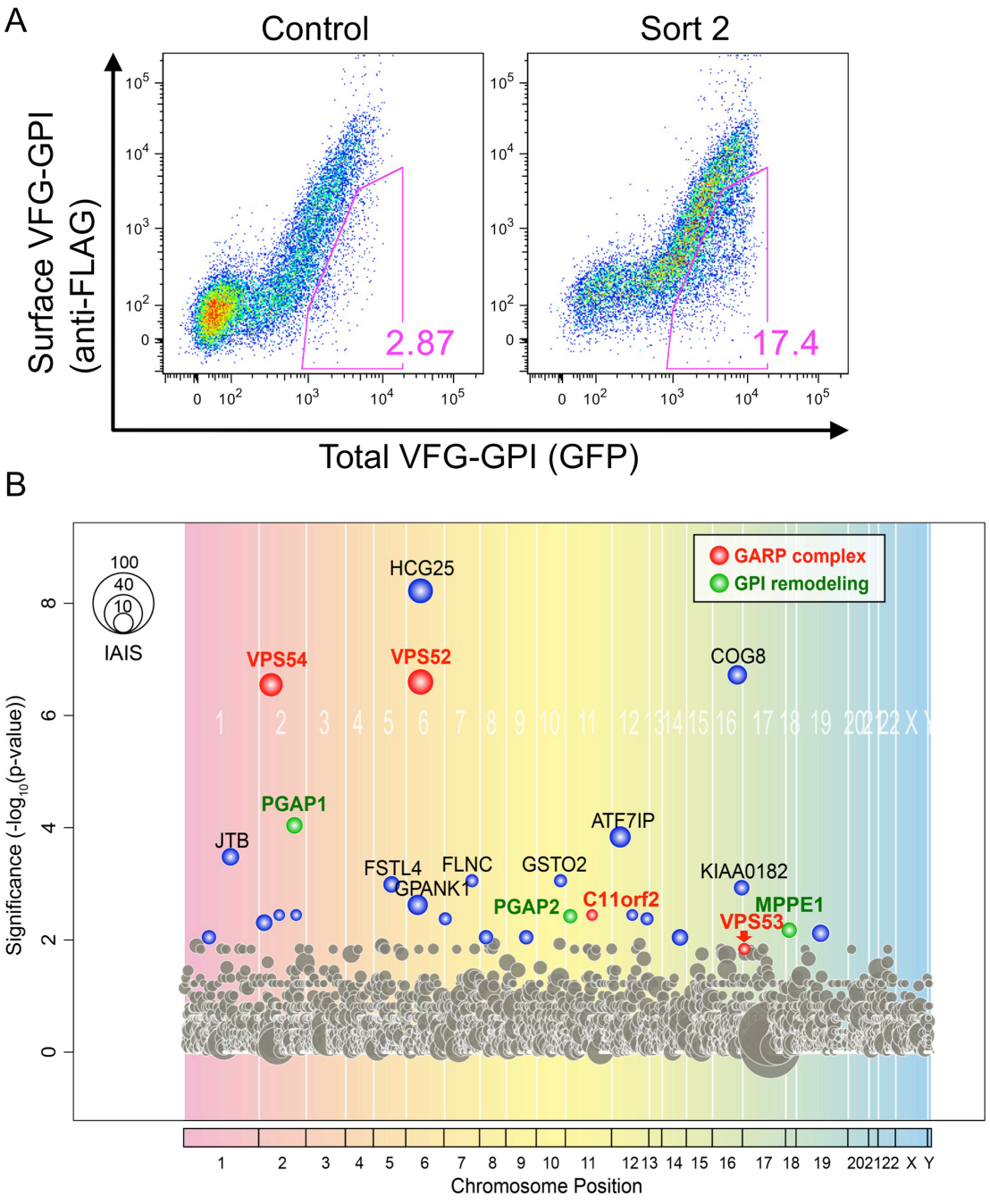
A
Control
Sort 2
Surface VFG-GPI (anti-FLAG)
Total VFG-GPI (GFP)
2.87
17.4
B
GARP complex
GPI remodeling
IAIS
HCG25
VPS54
VPS52
COG8
PGAP1
JTB
ATF7IP
FSTL4
FLNC
GSTO2
GPANK1
KIAA0182
PGAP2
C11orf2
MPPE1
VPS53
Significance (-log10(p-value))
Chromosome Position

Fig. 3

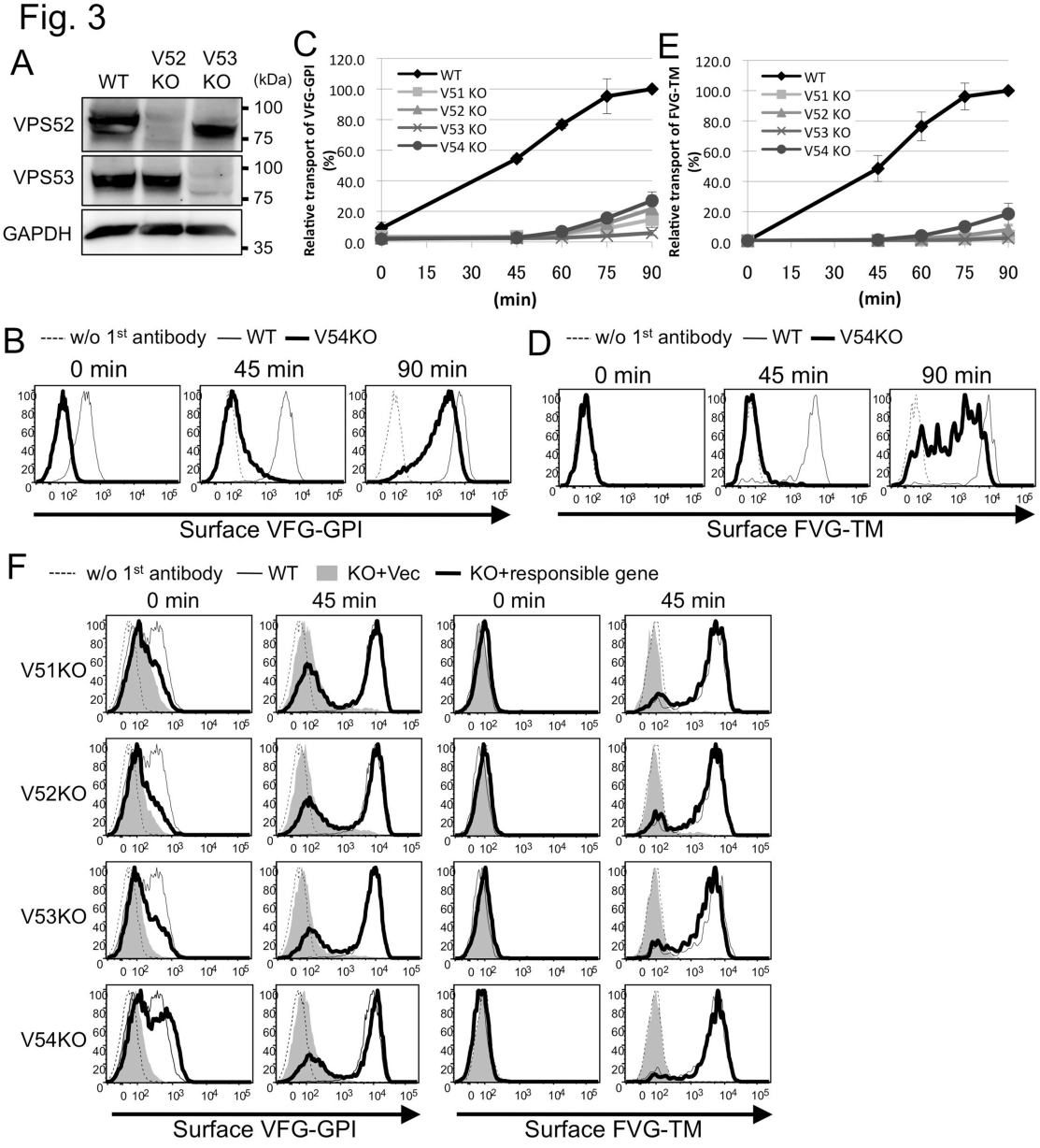
A
WT
V52 KO
V53 KO
(kDa)
VPS52
VPS53
GAPDH
100
75
100
75
35
C
Relative transport of VFG-GPI (%)
WT
V51 KO
V52 KO
V53 KO
V54 KO
(min)
E
Relative transport of FVG-TM (%)
B
---- w/o 1st antibody — WT — V54KO
0 min
45 min
90 min
Surface VFG-GPI
D
Surface FVG-TM
F
----- w/o 1st antibody — WT KO+Vec — KO+responsible gene
V51KO
V52KO
V53KO
V54KO

Fig. 4

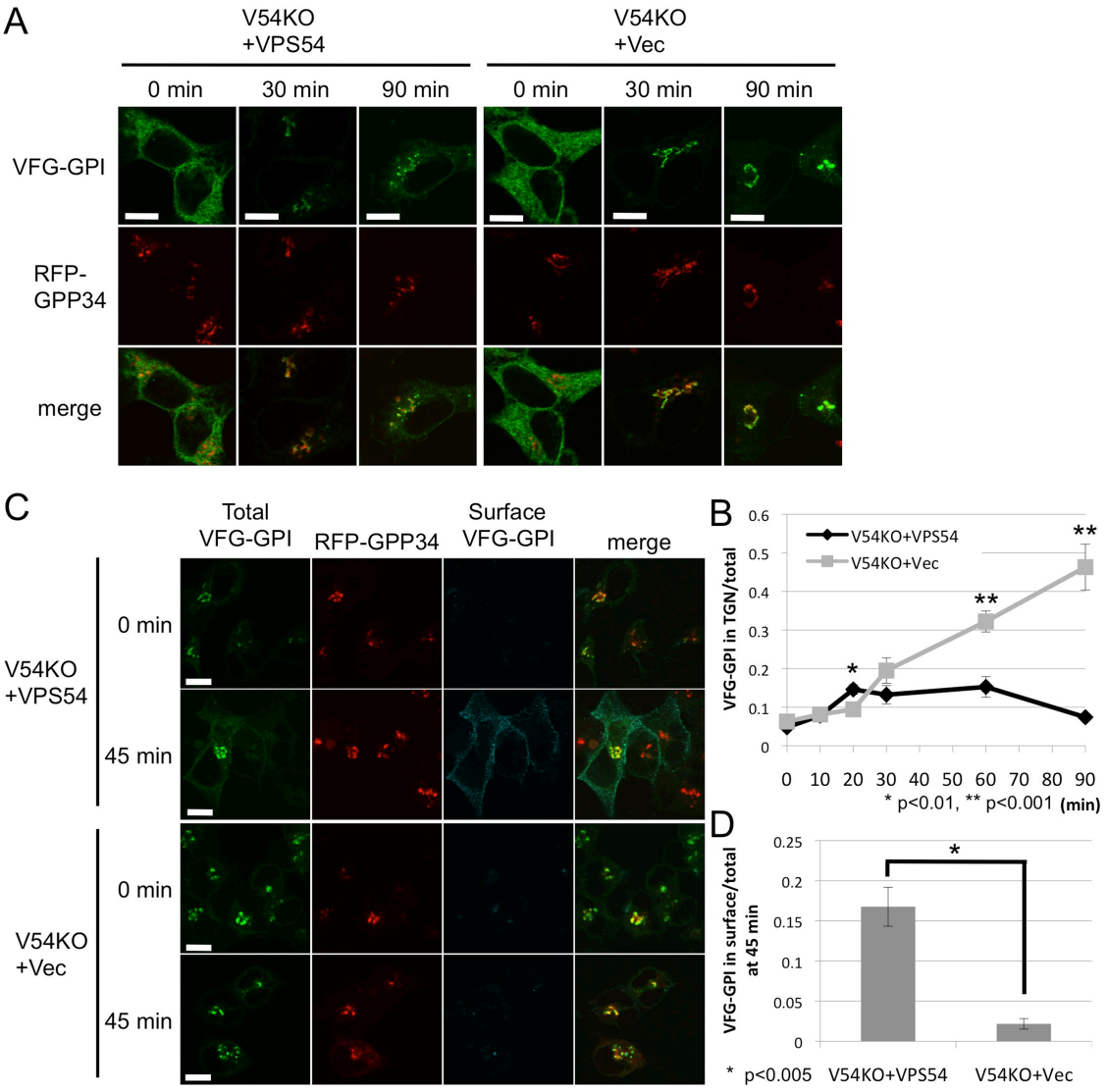
A
V54KO
+VPS54
V54KO
+Vec
0 min
30 min
90 min
0 min
30 min
90 min
VFG-GPI
RFP-
GPP34
merge
C
Total
VFG-GPI
RFP-GPP34
Surface
VFG-GPI
merge
V54KO
+VPS54
0 min
45 min
V54KO
+Vec
0 min
45 min
B
V54KO+VPS54
V54KO+Vec
VFG-GPI in TGN/total
0.6
0.5
0.4
0.3
0.2
0.1
0
0 10 20 30 40 50 60 70 80 90
* p<0.01, ** p<0.001 (min)
D
VFG-GPI in surface/total
at 45 min
0.25
0.2
0.15
0.1
0.05
0
* p<0.005
V54KO+VPS54
V54KO+Vec

Fig. 5

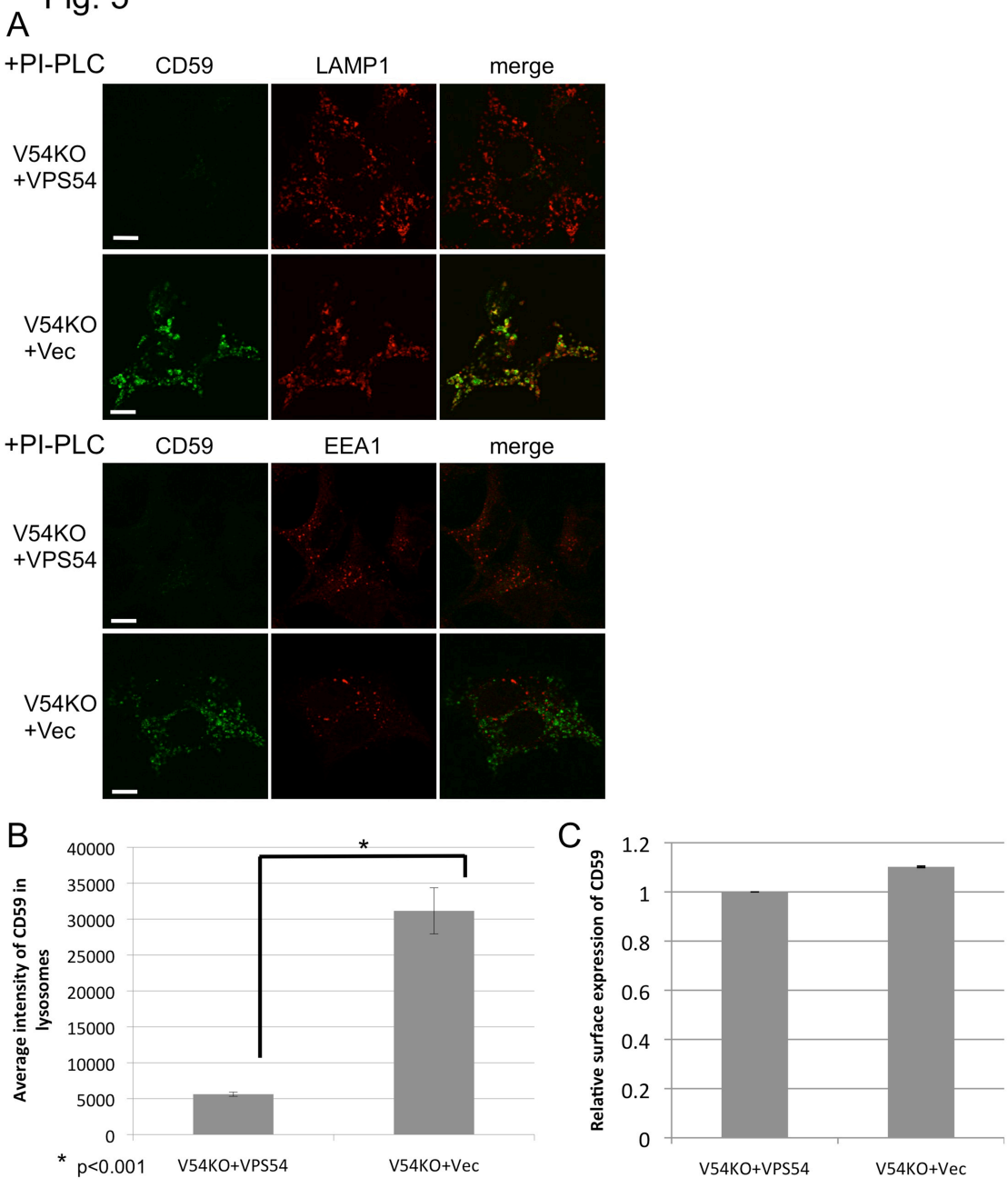
A
+PI-PLC
CD59
LAMP1
merge
V54KO +VPS54
V54KO +Vec
+PI-PLC
CD59
EEA1
merge
V54KO +VPS54
V54KO +Vec
B
Average intensity of CD59 in lysosomes
40000
35000
30000
25000
20000
15000
10000
5000
0
*
* p<0.001
V54KO+VPS54
V54KO+Vec
C
Relative surface expression of CD59
1.2
1
0.8
0.6
0.4
0.2
0
V54KO+VPS54
V54KO+Vec

Fig. 6

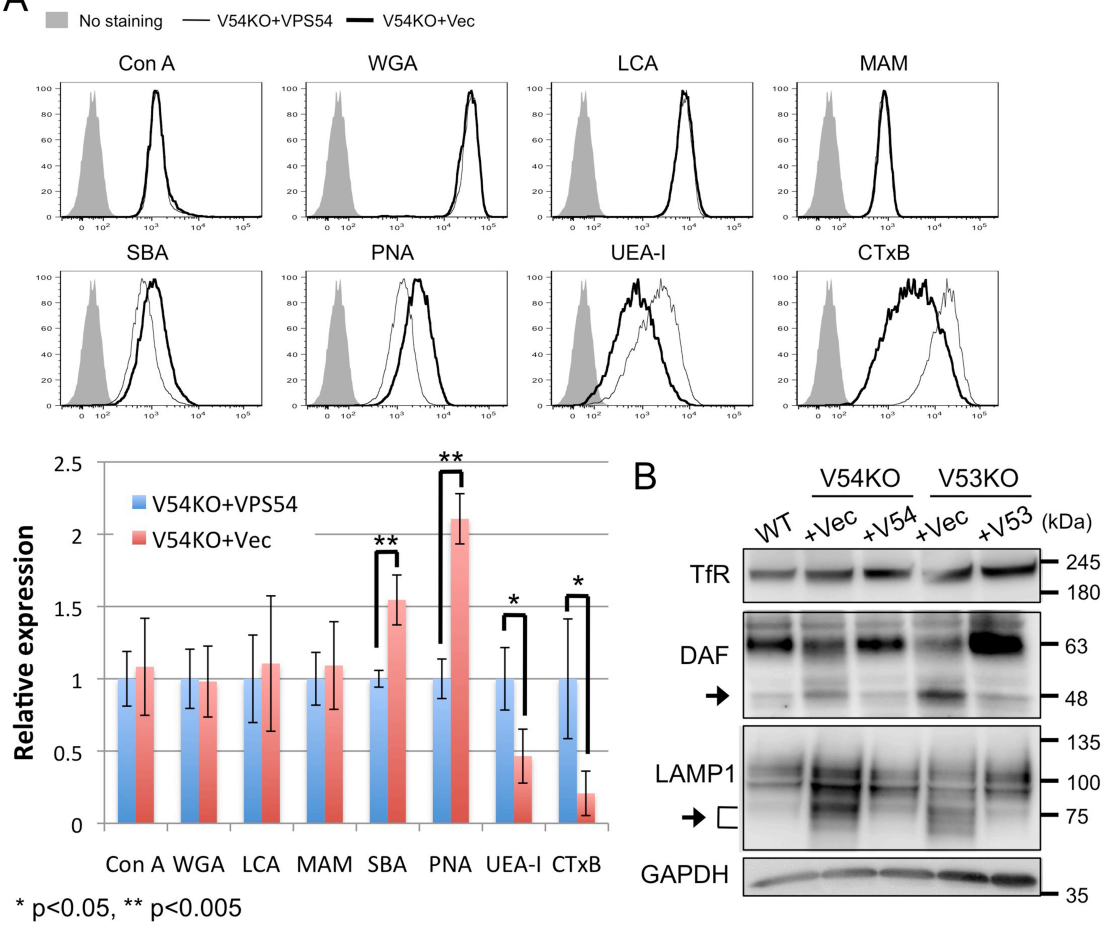
A
No staining
V54KO+VPS54
V54KO+Vec
Con A
WGA
LCA
MAM
SBA
PNA
UEA-I
CTxB
Relative expression
V54KO+VPS54
V54KO+Vec
Con A WGA LCA MAM SBA PNA UEA-I CTxB
* p<0.05, ** p<0.005
B
V54KO
V53KO
WT
+Vec
+V54
+Vec
+V53
(kDa)
TfR
DAF
LAMP1
GAPDH
245
180
63
48
135
100
75
35

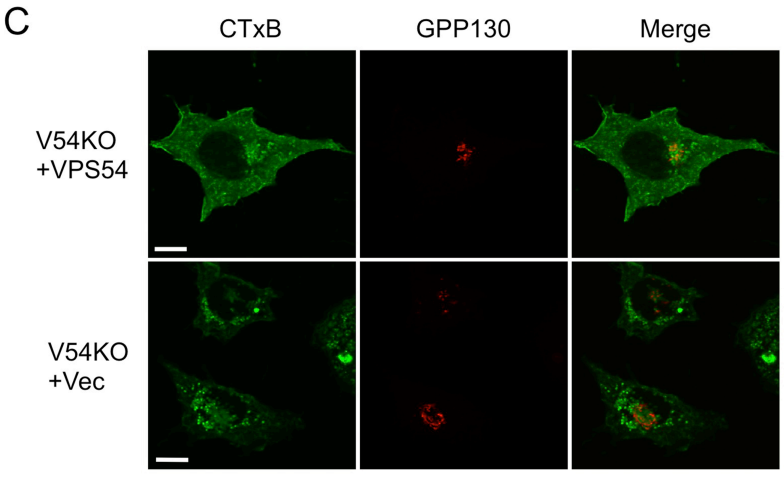
C
CTxB
GPP130
Merge
V54KO
+VPS54
V54KO
+Vec

Fig. 7

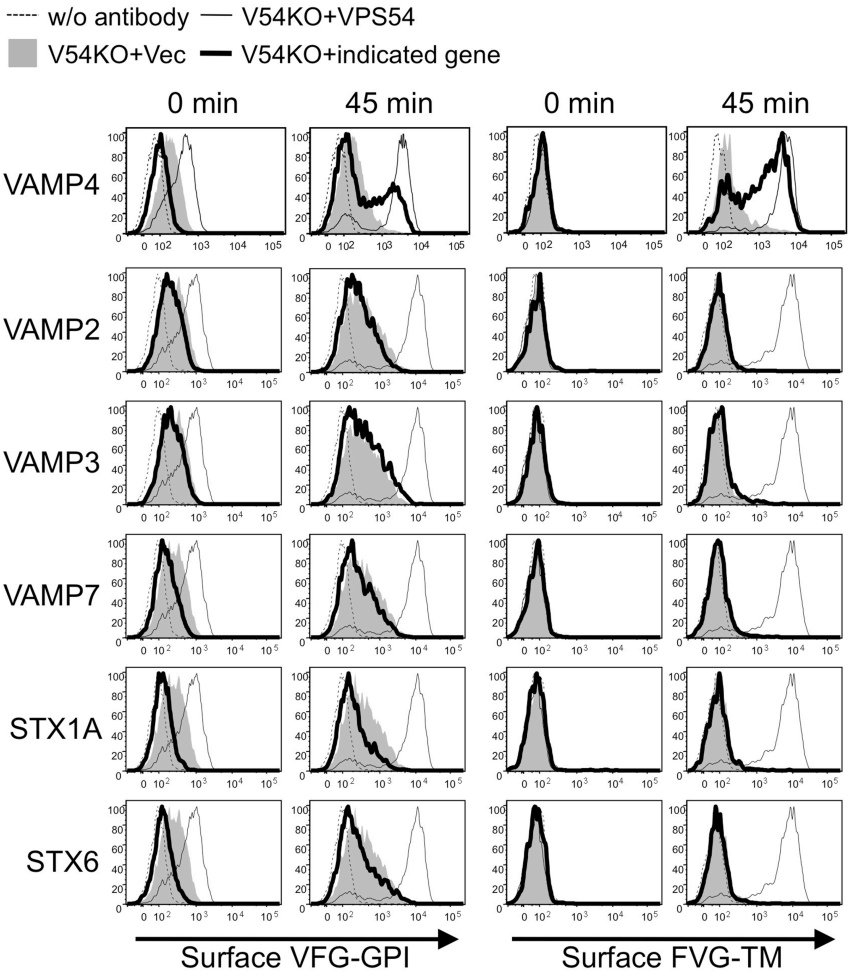
w/o antibody
V54KO+VPS54
V54KO+Vec
V54KO+indicated gene
0 min
45 min
0 min
45 min
VAMP4
VAMP2
VAMP3
VAMP7
STX1A
STX6
Surface VFG-GPI
Surface FVG-TM

Fig. 8

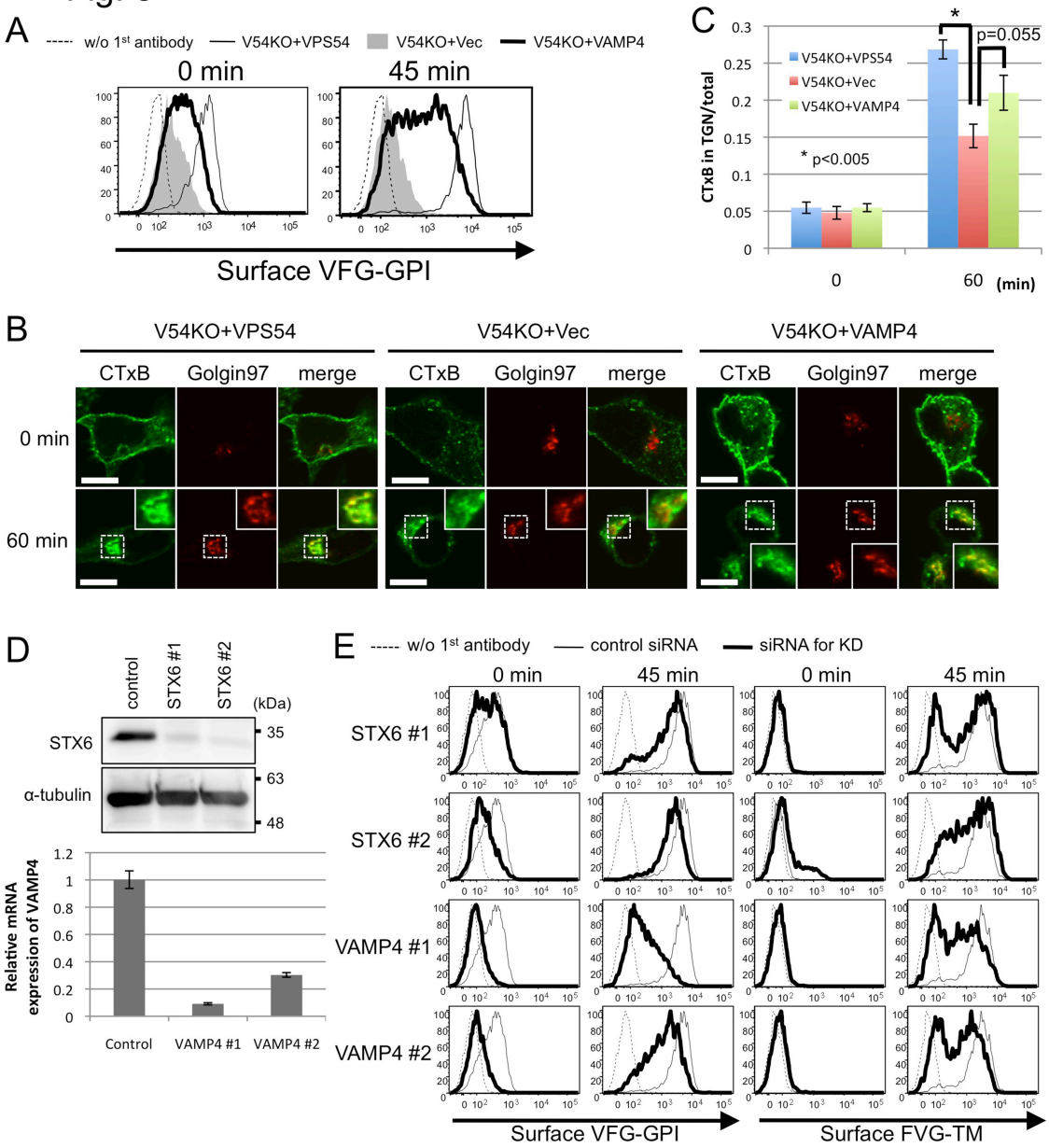
A
----- w/o 1st antibody
V54KO+VPS54
V54KO+Vec
V54KO+VAMP4
0 min
45 min
Surface VFG-GPI
C
CTxB in TGN/total
V54KO+VPS54
V54KO+Vec
V54KO+VAMP4
* p<0.005
*
p=0.055
0
60
(min)
B
V54KO+VPS54
V54KO+Vec
V54KO+VAMP4
CTxB
Golgin97
merge
0 min
60 min
D
control
STX6 #1
STX6 #2
(kDa)
STX6
α-tubulin
35
63
48
Relative mRNA expression of VAMP4
Control
VAMP4 #1
VAMP4 #2
E
----- w/o 1st antibody
control siRNA
siRNA for KD
0 min
45 min
STX6 #1
STX6 #2
VAMP4 #1
VAMP4 #2
Surface VFG-GPI
Surface FVG-TM

Fig. 9

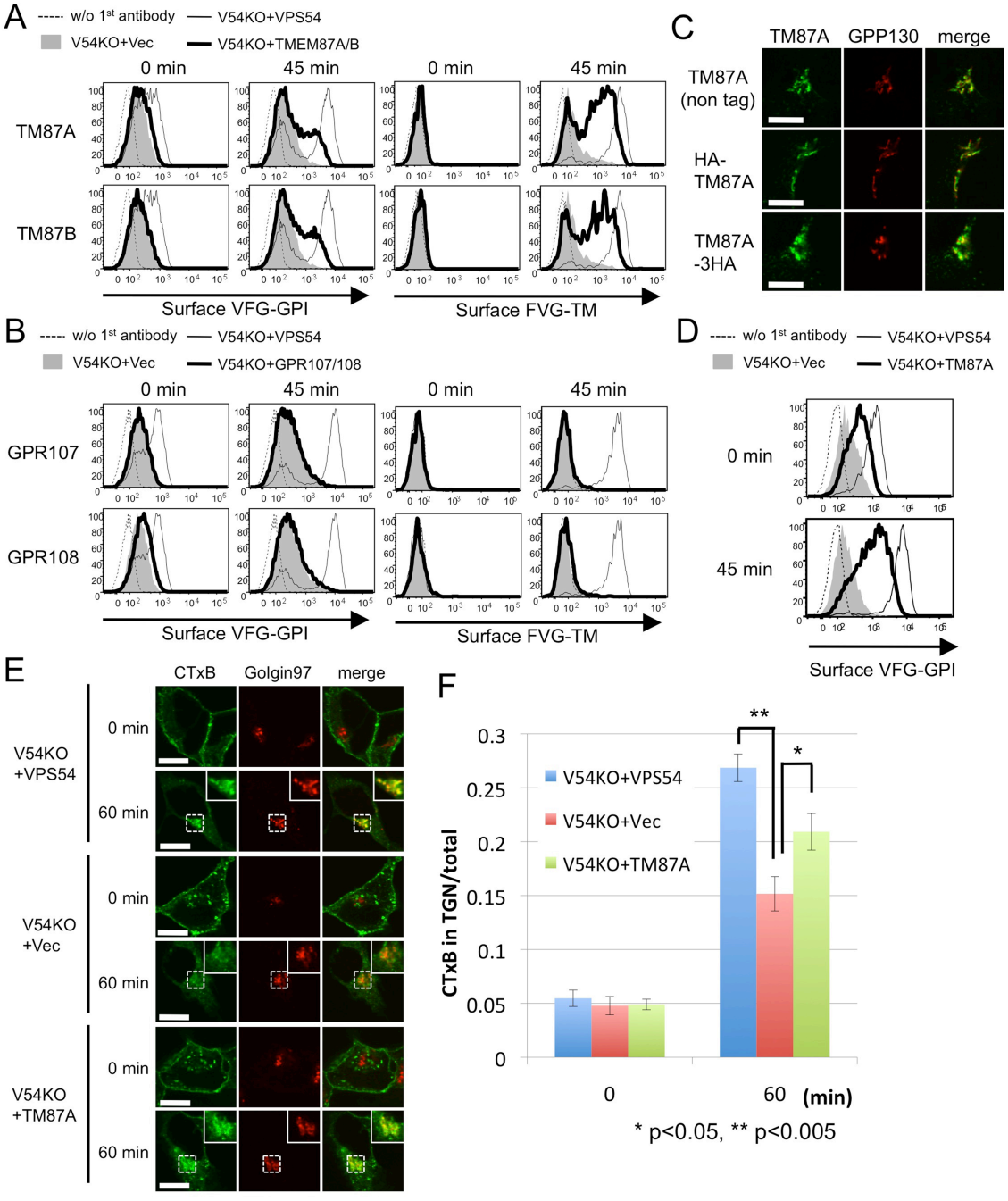
A
----- w/o 1st antibody
V54KO+Vec
V54KO+VPS54
V54KO+TMEM87A/B
0 min
45 min
0 min
45 min
TM87A
TM87B
Surface VFG-GPI
Surface FVG-TM
B
----- w/o 1st antibody
V54KO+Vec
V54KO+VPS54
V54KO+GPR107/108
0 min
45 min
0 min
45 min
GPR107
GPR108
Surface VFG-GPI
Surface FVG-TM
C
TM87A
GPP130
merge
TM87A (non tag)
HA-TM87A
TM87A -3HA
D
----- w/o 1st antibody
V54KO+Vec
V54KO+VPS54
V54KO+TM87A
0 min
45 min
Surface VFG-GPI
E
CTxB
Golgin97
merge
V54KO +VPS54
V54KO +Vec
V54KO +TM87A
0 min
60 min
F
V54KO+VPS54
V54KO+Vec
V54KO+TM87A
CTxB in TGN/total
0.3
0.25
0.2
0.15
0.1
0.05
0
0
60
(min)
**
*
* p<0.05, ** p<0.005

Fig. 10

A

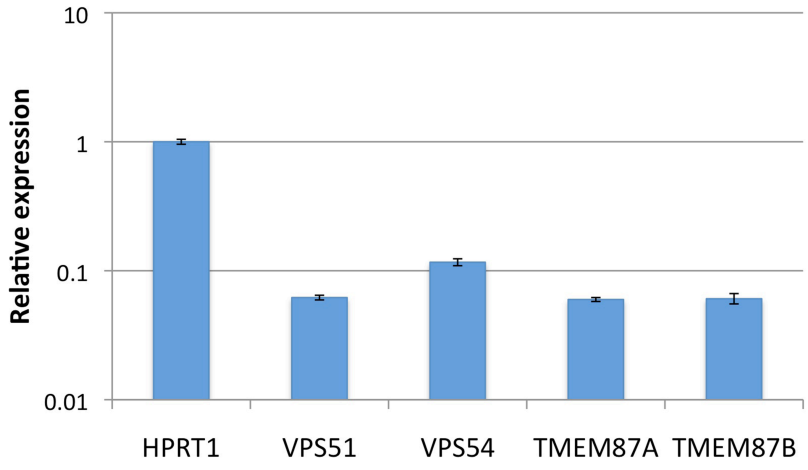
10
1
0.1
0.01
Relative expression
HPRT1
VPS51
VPS54
TMEM87A
TMEM87B

B

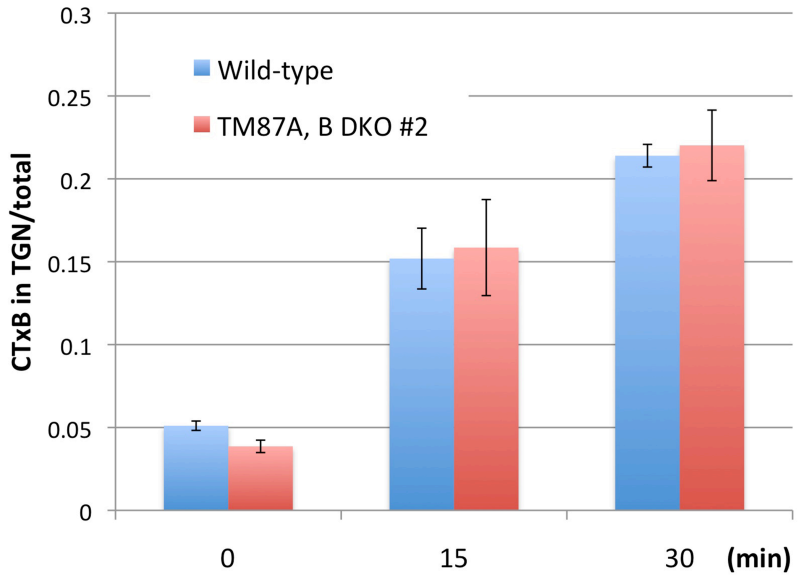
0.3
0.25
0.2
0.15
0.1
0.05
0
CTxB in TGN/total
Wild-type
TM87A, B DKO #2
0
15
30
(min)

Fig. 11

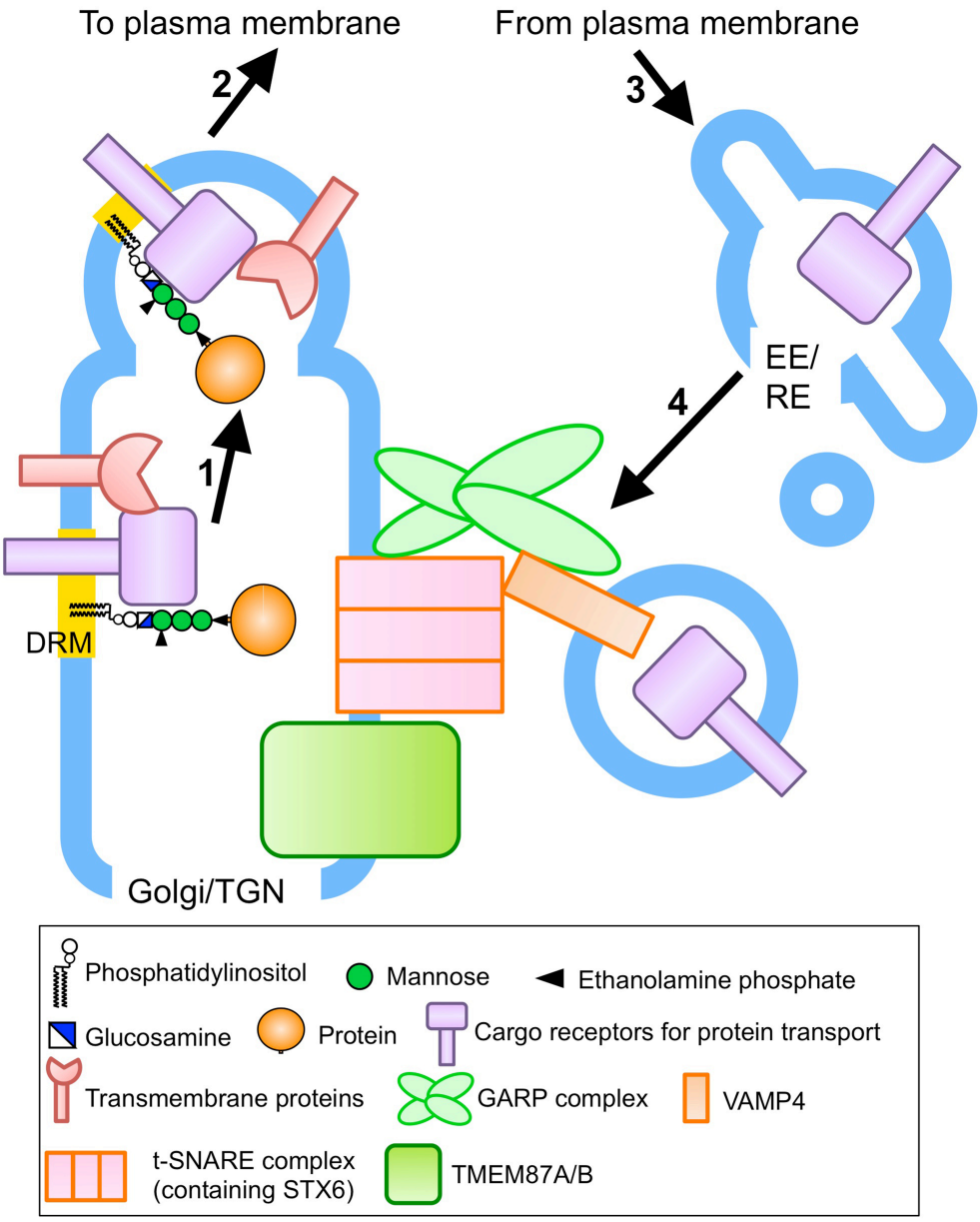
To plasma membrane
From plasma membrane
2
3
EE/
RE
4
1
DRM
Golgi/TGN
Phosphatidylinositol
Mannose
Ethanolamine phosphate
Glucosamine
Protein
Cargo receptors for protein transport
Transmembrane proteins
GARP complex
VAMP4
t-SNARE complex
(containing STX6)
TMEM87A/B

13. Publication and oral presentation in international conferences

Publication

1. Glycosylphosphatidylinositol mannosyltransferase II is the rate-limiting enzyme in glycosylphosphatidylinositol biosynthesis under limited dolichol-phosphate mannose availability

Tetsuya Hirata, Morihisa Fujita, Noriyuki Kanzawa, Yoshiko Murakami, Yusuke Maeda and Taroh Kinoshita

J. Biochem. 154, 3, 257-264, 2013

2. Post-Golgi anterograde transport requires GARP-dependent endosome-to-TGN retrograde transport

Tetsuya Hirata*, Morihisa Fujita*, Shota Nakamura, Kazuyoshi Gotoh, Daisuke Motooka, Yoshiko Murakami, Yusuke Maeda, and Taroh Kinoshita

Asterisk (*) represents equal contribution.

Mol. Biol. Cell, 26, 17, 3071-3084, 2015

3. Genome-Wide Screening of Genes Required for Glycosylphosphatidylinositol Biosynthesis

Yao Rong, Shota Nakamura, Tetsuya Hirata, Daisuke Motooka, Yi-Shi Liu, Zeng-An He, Xiao-Dong Gao, Yusuke Maeda, Taroh Kinoshita and Morihisa Fujita

PLOS ONE, 10, 9, e0138553, 2015

4. 3D structure and interaction of p24β and p24δ Golgi dynamics domains: implication for p24 complex formation and cargo transport

Masamichi Nagae, Tetsuya Hirata, Kana Morita-Matsumoto, Morihisa Fujita, Taroh Kinoshita and Yoshiki Yamaguchi

Submitting

Presentation in international conferences

1. Endosomes-to-TGN retrograde transport mediated by GARP is required for post-Golgi anterograde transport and glycosylation

Tetsuya Hirata, Morihisa Fujita, Shota Nakamura, Kazuyoshi Gotoh, Daisuke Motooka, Yoshiko Murakami, Yusuke Maeda and Taroh Kinoshita

Joint Meeting of the Society for Glycobiology and Japanese Society of Carbohydrate Research, Nov. 16th-19th, 2014

2. PGAP4, a multipass Golgi transmembrane protein, is a GPI-GalNAc transferase for generating GPI-anchor side chain

Tetsuya Hirata, Morihisa Fujita, Shota Nakamura, Daisuke Motooka, Noriyuki Kanzawa, Yoshiko Murakami, Yusuke Maeda and Taroh Kinoshita

23rd International Symposium on Glycoconjugates, Sep. 15th-20th, 2015